MONITORING ELECTRIC FIELD INDUCED CHANGES IN BIOLOGICAL TISSUES AND PHANTOMS USING ULTRASOUND

by

Jagdish Bhatt

Master of Physics, Tribhuvan University

Kathmandu, Nepal, 2004

A thesis

presented to Ryerson University

in partial fulfillment of the

requirements for the degree of

Master of Science

in the Program of

Biomedical Physics

Toronto, Ontario, Canada, 2015

Author's Declaration

I hereby declare that I am the sole author of this thesis. This is a true copy of the thesis, including any required final revisions, as accepted by my examiners.

I authorize Ryerson University to lend this thesis to other institutions or individuals for the purpose of scholarly research.

I further authorize Ryerson University to reproduce this thesis by photocopying or by other means, in total or in part, at the request of other institutions or individuals for the purpose of scholarly research.

I understand that my thesis may be made electronically available to the public.

Monitoring electric field induced changes in biological tissues and phantoms using ultrasound

Jagdish Bhatt

Master of Science, Biomedical physics

Ryerson University, 2015

Abstract

An external electric field can induce mechanical changes depending on the amplitude, frequency and duration of the applied electric field. This study is focused on monitoring the electric/electro-kinetic effects of real biological tissues (in vitro) and gelatin phantoms with high spatial resolution. In this study, we investigated the mean of the signal spectrum at the modulation frequency, root-mean-square of the noise in the spectrum, and signal-to-noise ratio (SNR) during the application of low-frequency AC electric field in tissues and phantoms. Our results show that the EIMC SNR can indicate the existence of AC electric current in samples, rather than be directly related to the sample's electro-kinetic properties of the samples. We also found that the SNR varies spatially even for homogenous samples. These two features might hinder the development of the proposed method to be a viable clinical diagnostic technique.

Acknowledgements

I would like to express my deepest gratitude to my supervisor, Dr. Yuan Xu for his inspired guidance, timely suggestions and continuous encouragement to pursue this study. I would like to thanks members of research committee Dr. Jahan Tavakkoli and Dr. Vladislav Toronov for their helpful suggestions and important advice during all the committee meetings.

I would also like to thank my family members, who were understanding and patient with me during the course of my study. I would also like to thank Ping Gong, Aditya Pandya and Ozkan Doganay for their assistance. Finally, I am grateful to all the staffs of the Physics Department who helped and supported me.

Table of Contents

List of Figures

Chapter 1

Introduction

1.1 Brief History of Diagnostic Ultrasound Imaging

Diagnostic ultrasound imaging has a wide range of medical applications such as abdominal, cardiac, maternity, gynecological, urological, breast and small tissue examination. It is an inexpensive, easy to use, mobile and non-ionizing medical imaging modality [3], [4] . Its popularity arises from the fact that it provides high-resolution images without the use of ionizing radiation [3]. The use of ultrasound in diagnostic imaging started shortly after the close of Second World War, derived from underwater sonar research [4]. In the beginning, the clinical applications monitored changes in the propagation of pulses through the brain to detect the brain tumors. The ultrasound imaging developed rapidly through the 1960s from "A-mode" (time/amplitude) imaging to "B-mode" (intensity modulation) applications. From the introducing of the gray scale processing of the signals in 1974, B-mode of the ultrasound imaging became popular. The progress in the development of the transducers has led to better resolution of very small structures in the abdomen [5].

The first real-time mechanical commercial scanner was designed by Richard Soldner in 1965. The machine consisted of a revolving transducer and a parabolic mirror which replaced the static B-scanners [5]. The progress changed the scope of ultrasound and it's applications in diagnostic radiology and medicine. Power Doppler, 3D data acquisition and the high resolution real-time imaging are the most important developments introduced into the clinical practice

[4].Ultrasound imaging is very useful for the diagnosis of the diseases of the coronaries, liver and prostate. However, this technique has a poor quality image, a lot of artifacts and a low signal to noise ratio. It is a very challenging task to get the useful information from the ultrasound data that makes the ultrasound imaging the active field of research [6].

1.2 The Physics of Ultrasound

Ultrasound is a mechanical wave at frequencies greater than 20 KHz that can propagate through different medium such as soft tissues, fluids, and bones. The medical ultrasound machines use the frequencies between 2 MHz and 15 MHz [7]. When the beam of ultrasound travels through the material, the particles of the medium oscillate around their mean position. The ultrasound waves interact with the material resulting in scattering and absorption. For a plane wave in a medium, the sound pressure p and the particle velocity v are related as follows**:**

$$p = \rho c v = Z v \ldots\ldots\ldots\ldots \quad (1.1)$$

where, ρ is the density of the medium, c is the speed of sound and $Z = \rho c$, is the acoustic impedance of the medium [8].

When the beam of ultrasound transmits through the material, the reflection and scattering of the incident wave can generate echoes. If the two materials have the same acoustic impedance then their boundary will not produce an echo. When the difference in acoustic impedance between the two boundaries is very high, a strong echo will be produced [9]. The intensity of the ultrasound beam can also be reduced by attenuation due to reflection, scattering and absorption. The reflection and refraction occur from the material surfaces that are large compared with the wavelength of the ultrasound. If the scatter sizes less than or equal to the wavelength of the

ultrasound wave then the energy is scattered in many directions. . The scattering of ultrasound gives a lot of diagnostic information that we observe in medical imaging [9], [10].

1.3 Electric field and biological tissues

Various methods were used to investigate the physical properties of biological tissues in medical imaging. The application of electric field on biological tissues is used to study the electrical properties of tissues such as conductivity and permittivity [11]. Many reports explaining the effects of electric field on biological tissues and its clinical applications have been reported. The mechanical change on biological tissues due to externally applied electric field is an important subject [12].

An externally applied electric field can also be used for manipulation of tissues and cells. The use of alternating electric field has been recently introduced for the treatment of glioblastoma (tumors found in cerebral hemispheres of the brain). The electric field distribution is highly non uniform and depends on the shape and dielectric properties of the tissues [13].

1.4 Motivation

Ultrasound imaging has been widely used for diseases screening and diagnosis purposes. It is relatively inexpensive and free of radiation risk and real time in nature when compared with other imaging technologies [5]. Ultrasound can also be used in dynamic study such that observing for pathological movement in tendon, muscles, or in joints and affected parts can be imaged in real time. At deeper structures, ultrasound imaging has a poor resolution however; recent advances in tissue harmonics have improved resolution and visualization of deeper structures [14]. The modern ultrasound is performed mainly using a pulse echo method with a

B-mode display. Usually only a small fraction of pulse returns as an echo after reaching a tissue surface partly scattered and partly absorbed [5].

The overall quality of the ultrasound image depends on many factors such as spatial resolution (axial and lateral resolution), temporal resolution and contrast resolution. Axial resolution is the ability to distinguish between echoes from two objects one behind the other along the axis of the ultrasound beam. Lateral resolution is the ability to distinguish two objects situated side by side perpendicular to the ultrasound beam. Temporal resolution is the ability to detect an object that has moved over time. The contrast resolution is used in medical imaging to measure the quality of the acquired images. It is the ability to distinguish between differences in intensity of an image [4]. The exact three dimensional imaging of biological tissues with high spatial resolution is important for the diagnosis. Ultrasound current source density imaging (UCSDI) is the technique which can be used to image the current flow in different tissues[15].

Ultrasound imaging is useful in characterizing tissue properties during electric field application. The mechanical response of the biological tissues during the physiological level electric field application can be investigated using ultrasound echo signal. The use of alternating electric field application to biological tissues to image the electric/electro-kinetic properties using ultrasound is a new research area. The tissue response can be monitored using ultrasound [16]. Noninvasive electrical impedance imaging methods have been actively investigated for decades because electric/electro-kinetic properties of biological tissues are sensitive to the physiological and pathological conditions of the tissues. These methods include magneto acoustic tomography, magnetic induction tomography, magnetic resonance electric impedance tomography and electric impedance tomography [17], [11].

The motivation of this research was to image the electric/electro-kinetic properties of biological tissues because the electric/electro-kinetic properties are correlated to the physiological and pathological status of the tissues. A new method of combining ultrasound with electric field to image the electro-kinetic properties of biological tissues will further improve the contrast of ultrasound imaging. The electric field induced mechanical changes (EIMC) on various biological samples of layered structures (muscle-fat-tissue) can be monitored to develop a new contrast mechanism of ultrasound imaging. It will be helpful to investigate more accurate diagnosis, earlier detection of diseases and characterization of the tissues based on electro-kinetic properties by measuring the change in amplitude of the echo signal from the layered structure during physiological level electric field application. In this study, the characterization of tissues and phantom based on the amplitude change of ultrasound echo signal under the application of electric field were performed in two different ways by using pork heart muscle, fat and the gelatin sample. Experiments were performed in both separating and without separating the tissues and phantoms using thin plastic (insulating material).

1.5 Organization of chapters

In this chapter we introduced a brief history of diagnostic ultrasound imaging, the Physics of ultrasound, a brief introduction of electric field and biological tissues and the motivation of this research. The second chapter includes the detailed literature review related to this research. The third chapter described the materials, methods used in this research and the terms used in this study. We presented the EIMC results and observations of the ex-vivo experiments in the fourth chapter. The last chapter includes discussion, conclusions and future work.

Chapter 2

Literature Review

2.1 Electrical conductivity

The conductivity of the biological tissues depends on the direction, and the frequency of the applied electric field. Biological tissues are inhomogeneous materials on a cellular scale with extracellular and intracellular space. The electrical conductivity of a tissue is inhomogeneous on a microscopic scale but on a macroscopic scale the conductivity of a tissue can be considered to be homogeneous which represents the electrical properties of the tissue averaged in space over many cells, and this conductivity is called the effective conductivity[18] . The measurement of the effective conductivity of the biological tissues is very important for understanding the tissues structures and functioning [19]. Most biological tissues display some characteristics of both insulators and conductors because they contain dipoles and charges. For a biological sample of thickness d and cross-sectional area A the conductance is given by the equation [20] which is

$$G = \frac{\sigma A}{d} \tag{2.5}$$

Where σ is the conductivity of the biological sample.

Some biological tissues are electrically anisotropic. For example, muscles are composed of fibers aligned in the direction of muscle contraction. The extracellular matrix is less conductive than the cell because electrical conduction along the length of the muscle fiber is easier than the conduction between the fibers in the extracellular matrix. Therefore, muscle tissue has typical anisotropic electric properties [20]. The conductivity measurement is very useful to identify the presence of tumor. Water is the better conductor of electricity than fat. Due to this reason the changes in the percentage of body fat or water are reflected in tissue impedance changes. Biological materials exhibit large difference in electric properties. For example, blood and brain conduct electric current relatively well. Lungs, skin, fat and bone are relatively poor conductors. Liver and muscle are intermediate in their conductivities [20], [21].

2.2 Electro-kinetic Phenomena

Electro-kinetic phenomena are a family of many different effects that occur in porous bodies filled with fluids, heterogeneous fluids or in a fast flow over a flat surface. Electro-kinetic phenomena (EKP) are the oldest area of surface and colloid science. The EKP such as electrophoresis, electro-osmosis, streaming potential and sedimentation potential has an important role in understanding of the colloidal science and the concept of electrical double layer [22], [23]. When the two uncharged phases are placed in contact a difference in electrical potential between the two phases is established. An essential requirement of EKP is the formation of an electrical double layer. Thickness of the electrical double layer ranges from several nanometers to hundreds of nanometers [24],[25].

2.2.1 Electrophoresis

Electrophoresis is the motion of the colloidal particles relative to a fluid under the action of the uniform electric field. It is due to the presence of the charged interface between the particle and the surrounding fluid. The electrophoresis of the positively charged particle is called cataphoresis while that of negatively charged particle is called anaphoresis. This method is frequently used in molecular biology and medicine for the separation and characterization of proteins and nucleic acids [26]. The insoluble solid which is dipped in an electrolytic solution forms a solid/liquid interface. The freely movable charge carriers can be adsorbed on the solid surface. In electrophoresis, the particles are separated based on their charge and size. An electric field is applied to the particles, and since the particles are electrically charged which results in force acting on the particles [1].

The greater the charge of the particle, the greater the force applied by the electric field and further the particle will move in the medium. A large sized particle will not move as far as the small particle with the same charge. The ratio of charge to mass of the particle determines how far it moves in the medium [23], [26]. During electrophoresis the particles are separated in a liquid and the electric field is applied by using the two electrodes as shown in Fig. 2.1 [1].

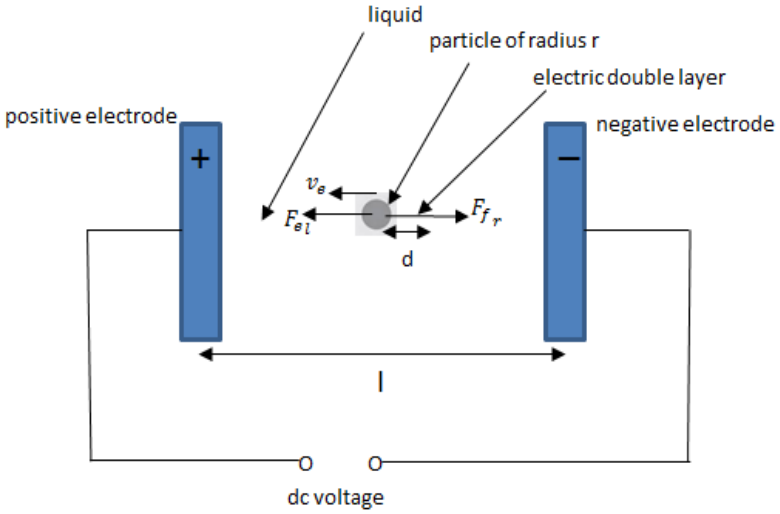

Figure 2.1: The detailed schematic of the principle of the particle electrophoresis [1]

When the electric force F_{e_l} is in the equilibrium with the friction force F_{f_r}, the particle having radius r moves with the constant electrophoretic velocity v_e .The electric field between the electrodes causes a particle movement. If E is the electric field strength, ζ is the zeta potential, ϵ_0 is the permittivity of the vacuum, ϵ_r is the relative permittivity of the liquid, U^{dc} is the applied direct current voltage, I is the distance between the two electrodes and η is the coefficient of viscosity of the medium then the electrophoretic velocity of the particles (v_e) can be calculated by using the equation [27] which is

$$v_e = \frac{-\epsilon_0 \epsilon_r E \zeta}{\eta} \tag{2.1}$$

The equation (2.1) is valid for the particles with $r << d$, where d is the thickness of the electrical double layer (EDL) [1], [27].The ratio of the electrophoretic velocity to the electric field strength is called electrophoretic mobility (u_e) which is

$$u_e = \frac{v_e}{E} \tag{2.2}$$

In the electrolytic solution the net charge on the particle surface affects the distribution of ions surrounding it. The region where the influence occurs is called the electrical double layer (EDL). The EDL consists of the two separate regions as stern layer and the diffuse layer. An inner region where ions are strongly bound is called stern layer and an outer region where the ions are weakly bound is called diffuse layer. The potential at the interface between stern layer and the diffuse layer is called the zeta potential which represents the electrical properties of solid/liquid and liquid/gas interface. The electric potential varies with the distance from the particle surface as shown in the Fig. 2.2.[2], [28]

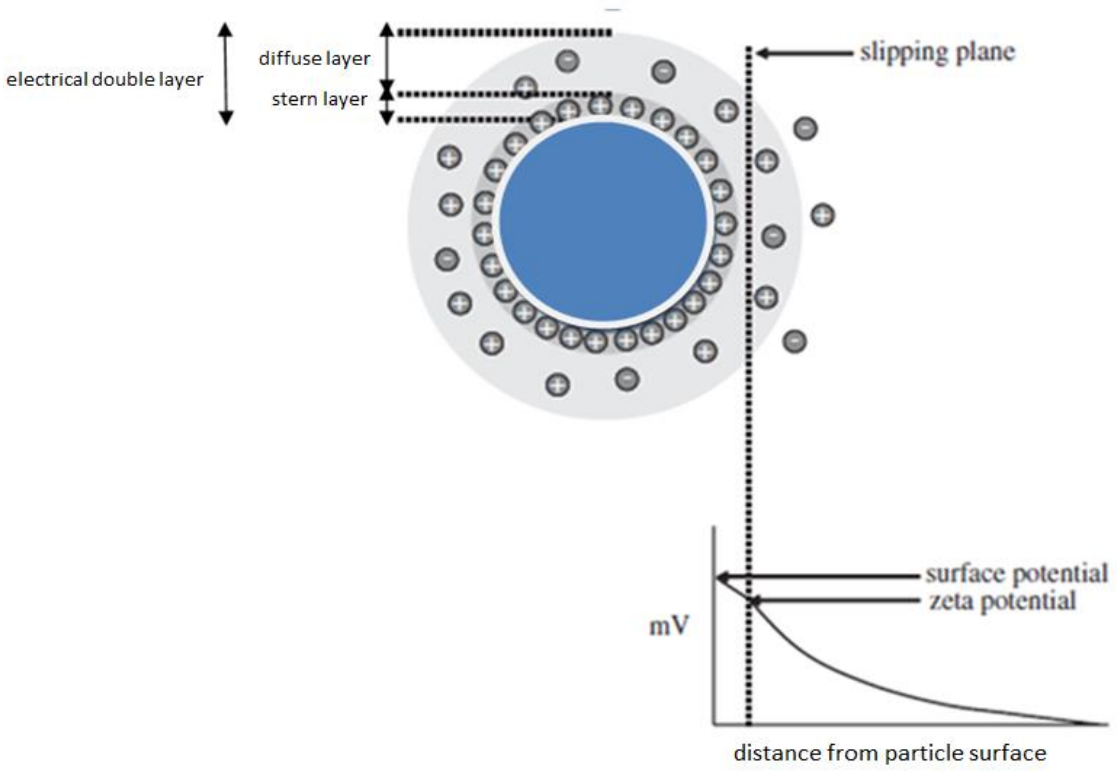

Figure 2.2: Schematic representation of the electrical double layer that surrounds a particle in an aqueous medium and the position of the slipping plane [2].

2.2.2 Electro osmosis

When electric field is applied across capillaries or micro channels, bulk fluid motion is observed. The velocity of the motion is directly proportional to the applied electric field and dependent on both the material used to construct the capillaries and the solution in contact with the capillary wall, this phenomenon is called electro osmosis. It is opposite to that of electrophoresis in which the liquid moves with respect to the solid particles under the action of electric field. Electro osmosis is applied in biological tissues to understand cell/tissue physiology because many biological tissues exhibit mechano-electrochemical phenomena such as ion induced swelling, streaming potential and electro osmosis [29]. In electro osmosis the thickness of the EDL is assumed to be very small compared with the particle radius. The electro osmotic slip velocity is given by the Smoluchowski equation [27] which is

$$v_{e_o} = -\frac{\epsilon_{r_s}\epsilon_0\zeta}{\eta}E \tag{2.3}$$

Where, ϵ_{r_s} is the relative permittivity of the electrolytic solution. The negative sign indicates the flow of liquid with respect to the solid.

An electric potential can be generated by the movement of the solid or liquid particles in a liquid when a charged particles move in a liquid medium under the action of some external forces is called sedimentation potential which is opposite of electrophoresis [1]. The streaming potential is produced when a liquid is forced to flow through a capillary or a porous solid medium. It is reverse of electro osmosis and depends on the presence of an EDL at a solid-liquid interface. This phenomenon is mainly due to the charge displacement in the electrical double layer as a result of an applied pressure [27].

2.3 Electric/electro-kinetic properties of biological tissues

The electric properties of biological tissue such as electric conductivity and permittivity play an important role in the diagnosis of various diseases, analysis of a wide range of biomedical applications and treatment of various physiological conditions with weak electric current [20]. A microscopic description of the response of a biological tissue to physiological electric field application is complicated by the variety of cell shapes and their distribution in the tissue. Therefore, a macroscopic approach is mostly used to characterize electric field distributions in biological tissues [20]. A few studies have been conducted on electrical properties of a cancerous tissue at various frequencies (10Hz-20GHz) and these studies have shown that the electrical properties of cancerous tissue are three or more times greater than those of healthy tissues [30]. Electro-kinetic properties contribute to the functions of many biological tissues and have practical applications in the control of molecular filtration. Fixed charge plays an important role in determining the functional properties of biological tissues and can be determined from the electro-kinetic responses of the tissues [31].

2.3.1 Fixed charge density in tissues

The fixed charge density (FCD) is a measure of the negative charges per unit volume in the extracellular matrix (ECM). The electrostatic interaction between mobile free ions and fixed charges results in electro-kinetic and physiochemical effects. The fixed charge density strongly affects the mechanical functioning of the tissue and it determines tissue osmotic pressure and hydration [32], [33]. An intervertebral disc (IVD) is a charged and hydrated soft tissue which consists of the nucleus pulposus (NP), the annulus fibrosus (AF) and cartilaginous end-plate. The fixed charges on the tissue results from the charged groups on glycosaminoglycan (GAG)

molecules on the proteoglycans (PG) found on the extracellular matrix of the IVD soft tissue. [33], [34]. The high fixed charge density generates osmotic pressure, streaming potential and other electrochemical phenomena and also contribute to the hydration and compressive strength of the tissue [35].

A new method of measuring the FCD in intervertebral disc tissue using the two point electrical conductivity method was developed. In this method the tissue is first confined and equilibrated in a potassium chloride (KCl) solution and the tissue conductivity was measured. The experiment was repeated with a different concentration of KCl solution and FCD was determined using the equation [33] which is

$$c^F = 2\sqrt{\frac{\chi^2_{c_1^*}\left[(c_1^*)^2-(c_2^*)^2\right]}{\left[\chi^2_{c_1^*}-\chi^2_{c_2^*}\right]} - (c_1^*)^2} \tag{2.4}$$

where c^F is the fixed charge density in the unit of mole of charge per unit volume of the tissue, $\chi^2_{c_1^*}$ and $\chi^2_{c_2^*}$ are the values for electrical conductivity of a tissue samples equilibrated in two different concentrations c_1^* and c_2^* respectively.

There are fixed charges on the bio-macromolecules (e.g. proteoglycans) on cell surface and extracellular matrix within biological tissues. Electric field induced mechanical changes (EIMC) on biological tissues are probably due to the following two mechanisms. The first mechanism is that cells and extracellular matrix deform due to the fixed charge in the solid phase of the tissues when subjected to electric fields. The second mechanism is due to the electro-osmosis phenomena [27] when the electric field is applied on the biological tissues. The electric field exerts a force on the excess of positive charges in the porous structure of the tissues. The water

in tissues can flow in a process known as electro-osmosis (due to the force exerted by the electric field on the counter charges in water). The electric force drives the water in the porous structures of the tissues as in the capillary tube. Both mechanical changes are determined by the fixed charged density in tissues. Since the changes in EIMC are mechanical in nature and they can be detected using ultrasound [36].

2.3.2 Local Environment (pH variations)

The electric/electro-kinetic properties of biological tissues are dependent on physical mechanism and the pH value. In biological tissues the important charge carriers are electrons, the positively charged hydrogen, potassium, calcium, magnesium and negatively charged phosphate ions. Those charges associated with proteins and extracellular matrix proteoglycans also contribute the tissue conductivity. The most important electrical properties of a biological membrane are electric charges, potential drop between the surroundings and the complex acid-base equilibrium of biological membrane [37]. The pH value of the normal and tumor large intestine cell membrane also depends on surface charge density [38]. At low pH values the positive surface charge density increases and at high pH values the negative surface charge density increases until a plateau is reached for both normal and tumor large intestine cells. Collagen contains nearly equal numbers of ionized amino and carboxyl groups and possesses little or no net fixed charges at physiological level of pH [37], [38].

In general, tumors are more acidic than normal tissues with average pH values of about 7.0 in tumors and 7.5 in normal tissues. The pH in tissue can be measured by insertion of pH electrodes. Probes for measuring pH in tissue have been designed with a tip diameter ranging from about 1μm to a few mm. Most of the electrodes are large compared with the diameter of the

cell and cannot easily be used to study the change in pH over small distances within tumors. Very fine electrodes have been made but are associated with a small signal noise ratio [39].

2.4 Ultrasonic properties of biological tissues

Biological tissues can be treated either as a varying density and compressibility or as a random distribution of scatters whose acoustic properties differ from the surrounding medium. Reflection occurs from the surfaces between tissues with different wave propagation properties (such as fat, muscle and blood). The degree of reflection depends on the acoustic impedance of the tissues. The remaining ultrasound energy may either penetrate deeper or be absorbed by the tissue [40]

Attenuation and scattering are important properties of tissue that contribute to diagnostic information in medical ultrasound. In B-mode imaging these tissue characteristics are extracted from variations in image brightness. The backscatter coefficient is commonly used to quantify the scattering properties of biological tissue. Measurement of this quantity includes the projection of a pulsed ultrasound beam into a volume of the tissue sample and monitoring echo signals due to scattering [41], [42]. If the ultrasound pulse encounters reflectors whose dimensions are smaller than the wave length of ultrasound or when the pulse encounters a rough, irregular tissue interface, scattering occurs because the process of absorption increases approximately in direct proportion to frequency [43].

For scatters much smaller dimension than the wavelength, the intensity of the scattered wave is proportional to the fourth power of the frequency of the incident wave and sixth power of the size of the scatters. In soft tissue, the density and the compressibility of scatters are similar to those in the surrounding medium. Thus, the contribution of scattering to overall attenuation is

very small. At low MHz frequencies, the attenuation by scattering in soft tissue is 10 to 15% of the total attenuation [8]. In clinical ultrasonic B-mode imaging, scattering of ultrasound by tissues plays a key role in visualizing the normal and abnormal tissue structures because gray scale B-mode images are formed by intensity modulating based on the amplitude of scattered signals [44]

The ultrasound attenuation in biological tissues varies approximately linearly with frequency as shown in the Fig. (2.3) [43].

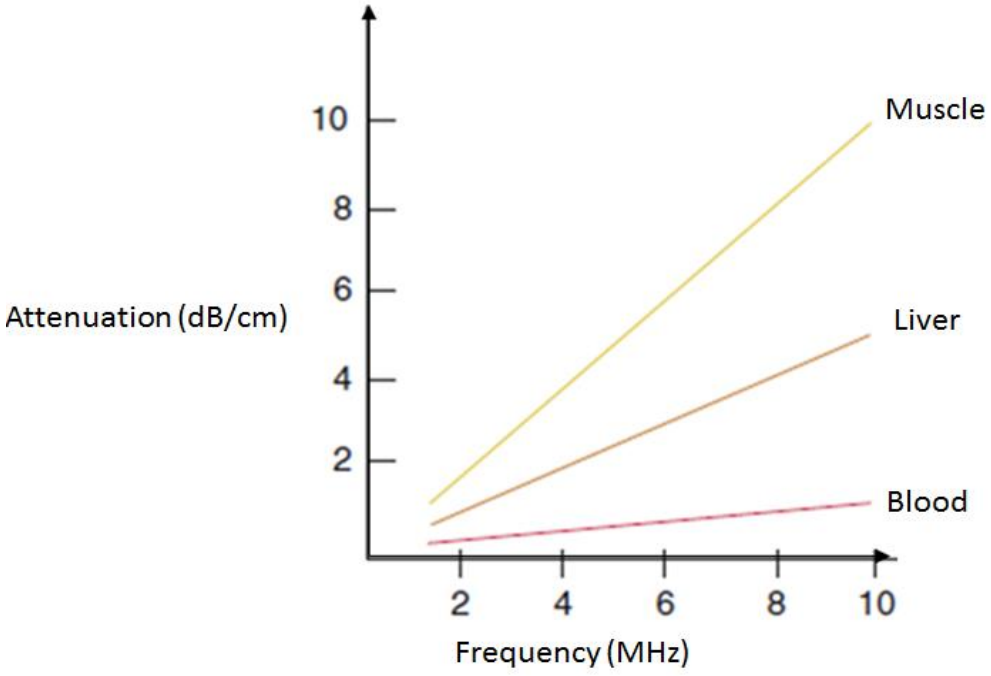

Figure 2.3: Degrees of attenuation of ultrasound beam as a function of the wave frequency in different biological tissues.

For soft tissues, this linear dependencies has been applied over a broad frequency range from 1 to 50MHz and for cancellous bone in a limited frequency range of 0.2 – 2MHz. Attenuation also

varies among body tissues, with the highest in bone, less in muscle and lowest in blood for any given frequency [8], [43]

2.5 Monitoring electro-kinetic response of biological tissues with optical coherence tomography (OCT)

Optical coherence tomography (OCT) is analogous to the ultrasound for imaging soft biological tissues. OCT uses light instead of ultrasound for imaging. OCT allows for high resolution, noninvasive and depth resolved imaging of internal tissue structure in micrometer scale at real time [45]. Amplitude changes of OCT signals were utilized to investigate the electro-kinetic phenomena in soft biological tissue. To investigate the electric field induced optical changes (EIOC), a Fourier transform was first applied to the detrended signal during the interval of electric field application. Then the magnitude of the spectrum at the frequency of the applied electric current [Fig. 2.4 (c)] was used to represent the magnitude of the EIOC image as shown in the Fig. 2.5 [46].

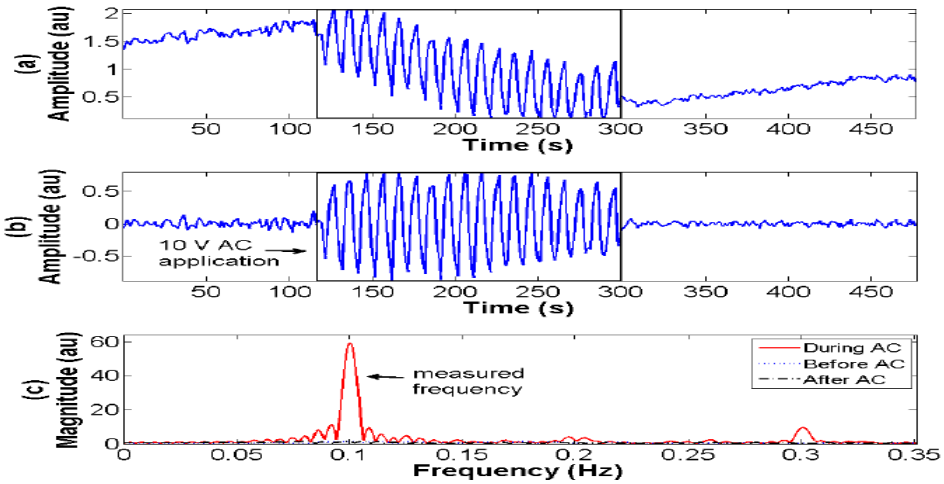

Figure 2.4 (a) the time course of a typical OCT signal acquired on a sample before, during (inside the solid square), and after the AC voltage application. (b) Same time course after detrending. (c) Fourier spectrum of 3 portions of the signal [46].

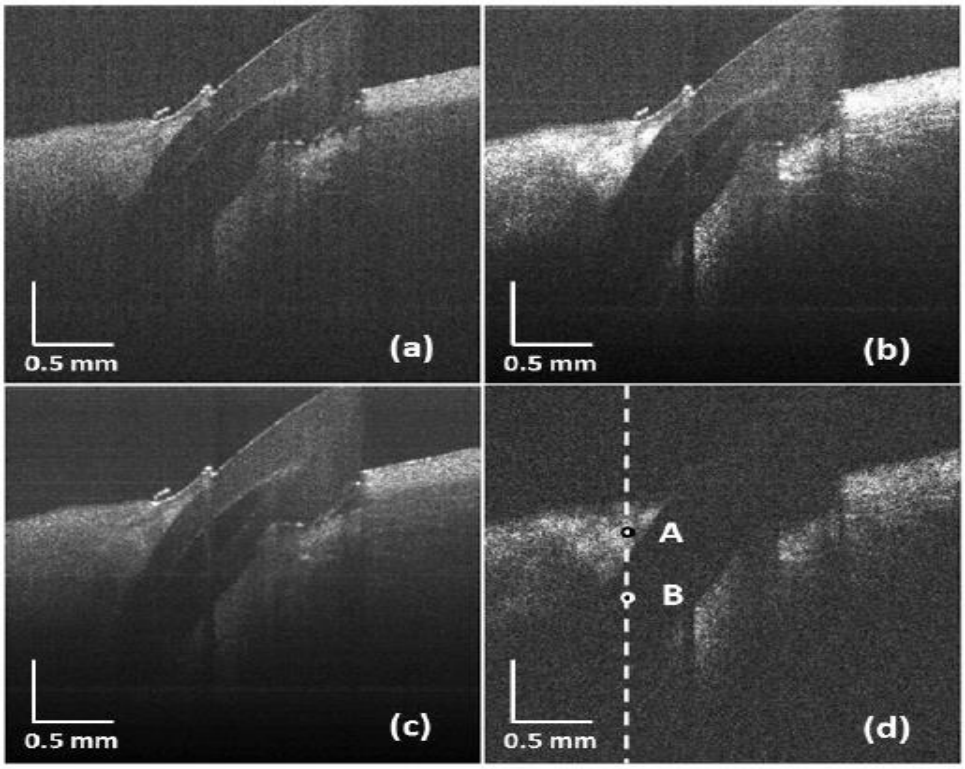

Figure 2.5: (a) Original OCT image (b) Un-normalized OCT-based EIOC image (c) EIOC background image during electric field application (d) OCT-based EIOC image normalized by the EIOC background image during electric field application.

A1 mm diameter dielectric optical fiber was inserted into the middle of the sample to verify the ability of the technique to image the electro-kinetic response of tissues [46]. Fig. 2.5 [46] (a) and (b) display the original OCT image and the un-normalized OCT based EIOC image respectively. In both Fig. 2.5 (a) and (b), the optical fiber material surrounding the transparent core can be clearly distinguished. Fig. 2.5 (c) display the EIOC background image during electric field application which was computed using the FFT magnitude averaged over all the frequencies except the narrow bands around $f_0=0.1Hz$ (applied frequency) and its corresponding harmonics. EIOC image was divided by the background image, pixel-by-pixel to find the normalised image as shown in the Fig. 2.5 (d). The normalised EIOC image represents the information related to

the electro-kinetic phenomena of the biological tissue. The fiber and a small piece of surface tissue to the left of the fiber in Fig. 2.5 (b) do not appear in Fig. 2.5 (d), which is in agreement with the absence of electric field in optical fiber. The amplitude of the OCT signal oscillates with the applied voltage [46],. The amplitude of the OCT signal oscillates with the applied voltage [Fig 2.4 (b)]; the similar trend was observed in the EIMC experiments studied in this research.

2.6 Hypothesis and objectives

Hypothesis

- Electric field can induce several mechanical changes in biological tissues and ultrasound phantoms depending on the duration of the applied electric field.
- Amplitude of the ultrasound echoes from the tissues can be monitored to reveal the current distribution in the sample.

Objectives:

- Study the electric/electro-kinetic effects in layered tissues (muscle-fat) and phantoms.
- Study the electric field induced mechanical changes (EIMC) based on the changes in the amplitude of RF signals, mean of the signal spectrum at the modulation frequency, RMS of the noise in the spectrum, and SNR during the application of electric field in tissues and phantoms.

Chapter 3

Materials and Methods

The methods used to analyze the electric field induced mechanical changes on biological tissues and phantoms using ultrasound is described in this chapter. In addition, more details on experiment protocol, tissue types used in this study and methods of data analysis are also discussed in this chapter.

3.1 Experiment setup

The schematic diagram for monitoring electric field induced mechanical changes on biological tissues using ultrasound is shown in Fig. (3.1) [12]. It consists of a function generator (Stanford Research System, model DS335), square wave pulser receiver (Panametrics – NDT, model 5077PR), ultrasound transducer, data acquisition card and two electrodes. The ultrasound transducer and the sample were immersed in the tank filled with mineral oil (Life Brand DIN 01935348). The transducer was fixed perpendicular to the surface of the sample in order to get the strong reflection from the sample.

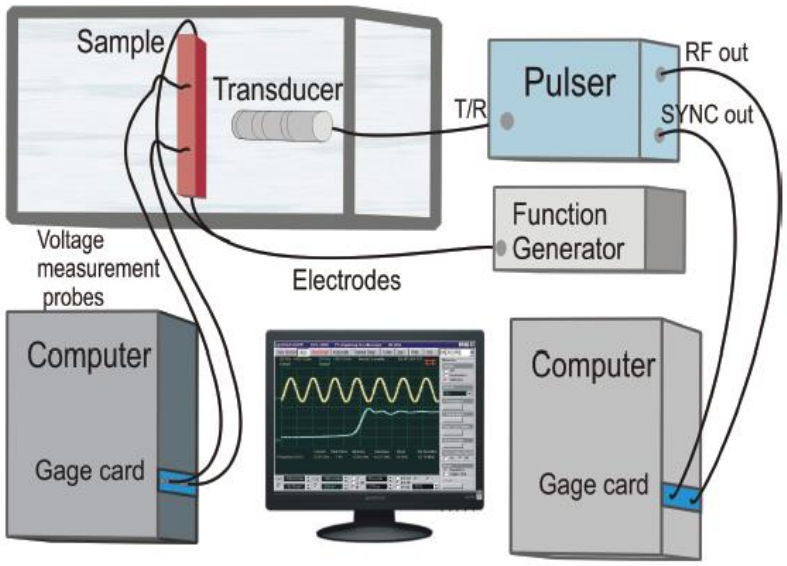

Figure 3.1: Schematic diagram of the experimental setup

The tissue samples examined in the experiments were at least 6cm×3cm×1cm. They were positioned in the plastic base to reduce the random mechanical motion of the sample. The longest dimension of the samples and the tissue fibers were positioned perpendicular to the ultrasound beam axis as shown in the Fig. (3.2) [36]. The electric current was applied to the tissue fibers through the copper electrodes separated by 5cm. Electrodes were kept in contact with the samples such that their terminals were across the longest dimension (across X-axis) as shown in the Fig. (3.2). This arrangement gave a relatively uniform electric field inside the tissue. For good coupling of the ultrasound waves, the tank was filled with mineral oil. All the experiments were carried out in normal room temperature.

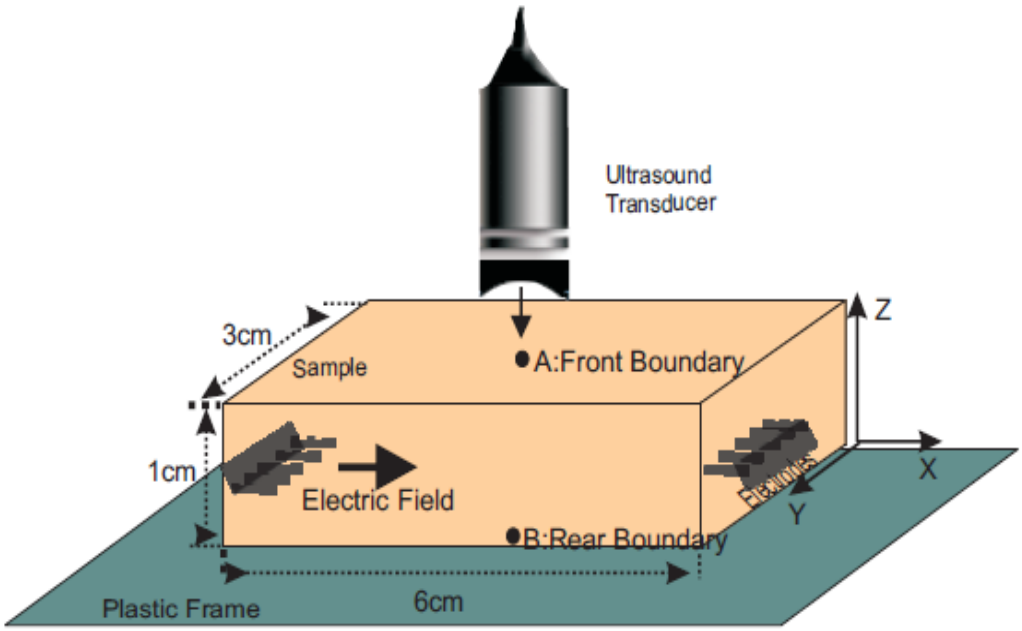

Figure 3.2: Schematic diagram showing the positioning of the sample and the ultrasound transducer during electric field application.

The electric current was applied to the sample by a synthesized function generator. Ultrasound pulses were transmitted and received by a 10MHz spherically – focused immersion transducer of focal length 1.9cm. The transducer was placed very close (1cm to 2cm) to the top surface of the sample in order to constantly acquire RF data. The diameter and the focal zone of the transducer were 1.3cm and 0.3cm. The pulser receiver produces an electrical pulse to excite a transducer that converts the electrical input to mechanical energy, creating an ultrasonic wave. The pulser receiver features adjustable voltage and repetition rate. In the experiments, the ultrasound was focused at the middle part of the sample, which has a relatively uniform current density. Ultrasound travels through the sample along Z-axis until it is reflected from an interface back to the transducer. The transducer reconverts the mechanical pulse into an electrical signal. The

resulting ultrasound echo signals (A-lines) from the sample were sampled at the sampling rate of 200MHz by a 14-bit data acquisition card and then stored in the computer for further processing.

3.1.1 Experiment Phantoms

A tissue-mimicking phantom follows important properties of biological tissues for the purpose of providing a more clinically realistic imaging environment. Depending on the imaging modality, certain physical and ultrasonic properties are of critical importance when making a tissue-mimicking phantom. In the case of ultrasound imaging, the most important properties are the speed of sound, attenuation coefficient and acoustic backscattering coefficient. In soft tissues, the speed of sound is 1540m/s and the attenuation coefficient ranges from 0.5 to 3.3 $dBcm^{-1}MHz^{-1}$.The backscatter coefficient ranges from 10^{-5} to $10^{-1}cm^{-1}Sr^{-1}$. The acoustic attenuation and the backscattering coefficient depend on frequency. The primary component of the ultrasound phantom tends to be water based (for example gelatin) which results in a speed of sound similar to biological tissue [47]. For this study, we used animal tissue types (porcine heart muscle and porcine fat) which were available from local grocery store (Fu Yao Supermarket) and the gelatin phantoms as shown in Fig (3.3) and (3.5).

Figure 3.3: Porcine heart muscle and gelatin sample

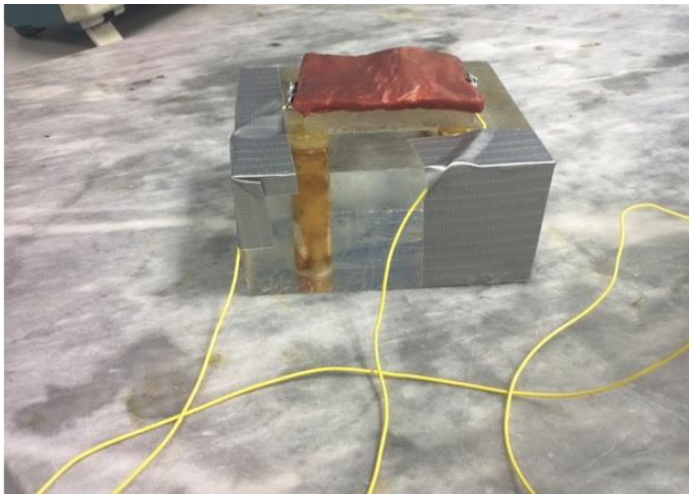

Figure 3.4: Porcine heart muscle fixed with electrodes and placed on the top of the gelatin sample

Figure 3.5: Porcine heart muscle, porcine fat and the gelatin sample.

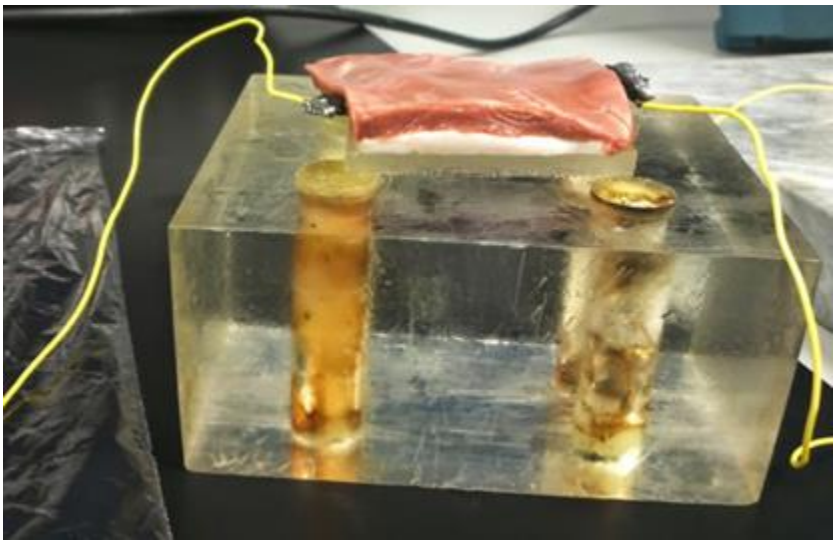

Figure 3.6: Porcine heart muscle fixed with electrodes and placed on the top of the porcine fat tissue.

Gelatin sample

Gelatin sample for ultrasound experiment was developed after reviewing the studies [48] and [49]. In order to prepare the gelatin sample, de-ionized water was used. A gelatin powder of 7.5gram (gelatin from porcine skin, Sigma Life Science, product code 1000612021) and the

scattering material (polyethylene oxide, Aldrich, 181994-250G) of 3gram was added to the 150ml de-ionized water. The scattering material was suspended in the medium to produce the backscatter that makes ultrasound imaging possible. The mixture was constantly stirred. The mixture was slowly heated up to 60°c to 70ºc over the course of 10 to 15 minutes. Application of heat was turned off after a clear solution was seen indicating the dissolution of gelatin and the scattering material in the de-ionized water. After mixing, the phantom was allowed to cool and placed into a 4°c refrigerator for 24 hour to allow the solution to fully cross-link. Care was taken to avoid formation of bubbles while mixing. Experiments were then performed on the samples.

3.2 Important terms used in this chapter

Slow time (s) – Slow time is the instant when the ultrasound transducer was triggered and was also used to describe the time line of the application of the voltage source to the sample. The slow time was on the order of seconds.

Fast time (µs) - The fast time represents the arrival time of the ultrasound echoes, which was the interval between the triggering of ultrasound transducer and the received echoes. The fast time is related to the thickness of the sample in the Z-axis in terms of the travel time of the ultrasound echo from the sample. The fast time scale was on the order of microseconds.

Amplitude change (V) – The changes observed in amplitude of windows induced by the application of AC electric field.

Mean signal (V) - The mean amplitude of the frequency spectrum at 0.02Hz was calculated and represented as the mean signal.

Root mean square noise (V) - The root mean square of the amplitude of the spectrum between the frequencies 0.05Hz and 0.25Hz was obtained and represented as the noise in the signal.

Signal-to-noise ratio (SNR) – The ratio of the mean amplitude of the signal of interest to that of the noise is called the signal-to-noise ratio (SNR).

3.3 Experiment Protocol (Data Acquisition)

The effects of electric current on biological tissues were studied for AC voltage of 8 volts and frequency 0.02Hz for various time intervals (1014s, 1059s and 381s). We choose 0.02 Hz because the EIMC effect decreases inverse proportional to the frequency. We have to choose a low frequency to obtain signals with good SNR. Before the electric current was turned on, 300 – 500 acquisitions were obtained to serve as the base line to check the system stability. This interval also provides information about background fluctuations due to small vibrations of the building and experiment table. Each A-line comprised of 14972 sampling points and a single acquisition took 0.588s (60s/102). The sampling rate of acquisition for experiments with single element transducer was 200MHz which translates to a sample spacing of 5ns. The pulsing device selected for this data acquisition system was a panametrics 5077PR. This is an ultrasonic square wave pulser/receiver unit. The algorithm developed used interpolation to estimate the time delay estimates. All the samples of biological tissues (porcine heart muscle and porcine fat) used in this study were from local grocery stores.

3.4 Sample for experiments

In this study, the experiments were performed by using the insulating material (plastic) between the samples and without the plastic between samples. A constant AC electric field was applied in the sample during the experiments for different time intervals.

(a) Gelatin layer electrically isolated from tissue layer

- Shorter time experiment using porcine heart muscle and gelatin sample separated by thin plastic
- Longer time experiment using porcine heart muscle and gelatin sample separated by thin plastic

(b) Gelatin layer in contact with tissue layer

- Longer time experiment using porcine heart muscle and gelatin sample without using plastic between samples
- Longer time experiments using layered tissues and phantoms (porcine heart muscle, fat and gelatin) without using plastic between samples

(c) Single gelatin experiment

3.5 Data Analysis

In order to study the electric field induced mechanical changes on biological tissues and samples, the ultrasound echo signals were acquired continuously in a pulse mode during the application of electric field with the transducer fixed at one position perpendicular to the surface of the sample.

Some small windows were chosen in the ultrasound signals. The peak-to-peak values of the signals were used to represent the signal amplitudes and the flight times of peaks were used to represent the phases in each individual window. In this study, the time domain amplitude change signal of all the windows in the echo signal from the sample was transformed into a frequency domain and then mean signal and the root mean square of the noise was observed to analyze the fluctuations in signal-to-noise ratio for whole sample during electric field application. The comparison between experiments with and without the plastic membrane between samples during electric field application shows some significant difference.

3.5.1 Amplitude change in various windows with slow time

In order to find the amplitude changes of the collected ultrasound echo signals due to electric field application, the windows were chosen in the A-mode signal as shown in Fig (3.7) [12].

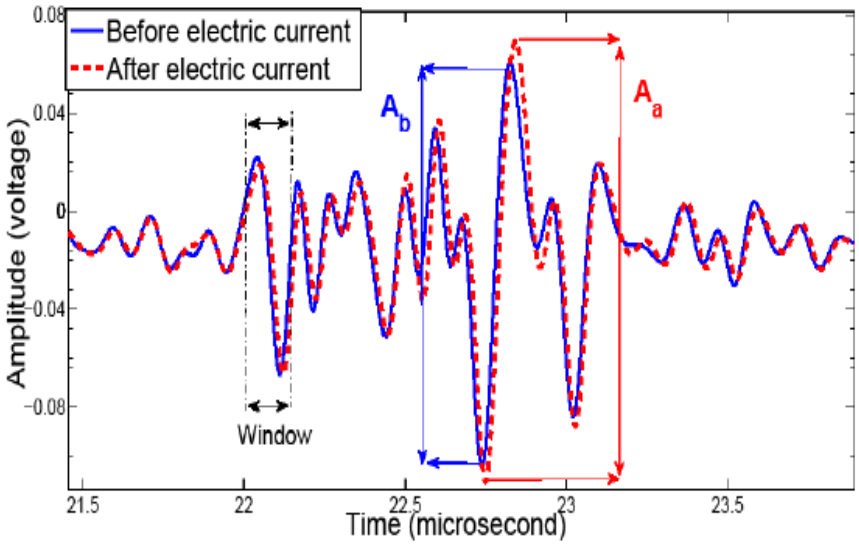

Figure 3.7: The echo signal from a piece of bovine muscle tissue before and after electric field application.

Fig. (3.7) shows the portion of the ultrasound echo signal from a piece of bovine muscle before (solid line) and after (dotted line) applying a DC voltage of 10 volts for 40 seconds to the tissue. A_a and A_b represents the peak-to-peak value of the signal within a small window after and before the application of electric field to the tissue. During the application of electric field the amplitude increases in some windows and decreases others as shown in the Fig. (3.7).

Each window size is about one wavelength, covering one peak and one valley of the echo signal. Using the maximum and minimum valus of the each window, amplitude changes were measured by usng an algorithm in matlab to find the peaks within the windows and observing the changes occuring in the peak to peak amplitude as a function of slow time. The changes are then monitored over a long period of time starting from the beginning of data acquisition to the end of data acquisition as shown in Fig. (3.8).

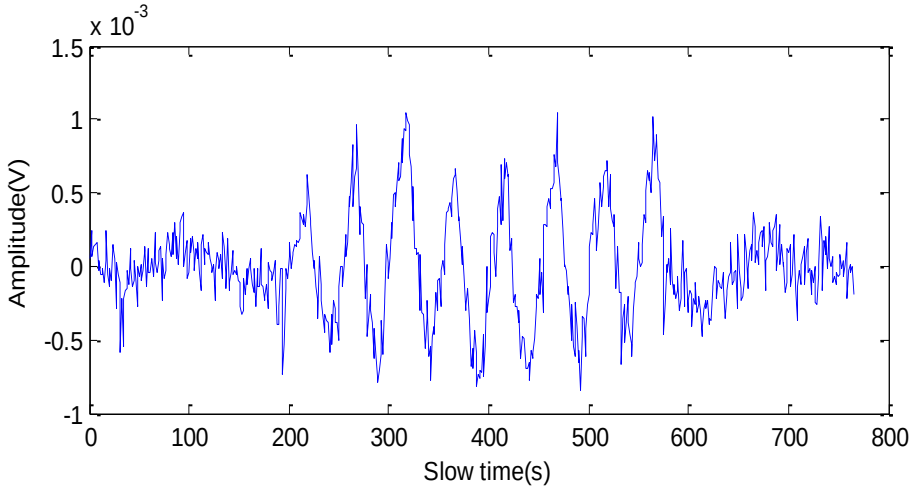

Figure 3.8: The amplitude change of a porcine heart window during the AC electric field application (1.33V/cm and 0.02Hz) for 381s. The current applied from 191s to 572s.

In this study, the change in amplitude of the windows in the porcine heart muscle, porcine fat and the gelatin sample before, during and after the application of the AC electric field (1.33V/cm, 0.02Hz) were obtained with the slow time. The amplitude change in the windows of the gelatin sample were also plotted with the slow time to check how much amplitude would change even though the gelatin sample has no electric field application. The electric field was applied for both longer time and the shorter time experiments to analyze the change in amplitude of the windows in the whole sample.

3.5.2 Analyzing the frequency spectrum of the signal during electric field application

The signal was selected during the electric field application as shown in Fig. (3.9). The Fourier transformation was applied to find the frequency spectrum of a signal as shown in Fig. (3.10) and to analyze the change in amplitude of the window. Since, it is difficult to identify the frequency component by looking at the original time domain signal. Converting time domain signal to frequency domain signal, the Discrete Fourier Transform (DFT) of the signal was found by taking the Fast Fourier Transform (FFT) using the code developed in Matlab. FFTs produce the average frequency content of a signal over the entire time that the signal was acquired and the amplitude of the FFT is related to the number of points in the time-domain signal.

In order to get the frequency spectrum of the signal during electric field application, a certain length of the detrended time domain signal was selected. Fourier transformation was applied by using the "fft" function in Matlab to the detrended signal to get the spectrum amplitude of the required signal during current. In this study, experiments were performed for longer and shorter time durations using porcine heart muscle and gelatin sample where gelatin sample was electrically isolated using a thin plastic. The detrended signal which was used to apply for

Fourier transformation has different number of points in the signal for shorter and longer duration during electric field application which causes the length of the signal was smaller for shorter time and larger for longer time durations (length of the signal (L) = $n\Delta t$, where n is an integer and Δt is the sample interval). The frequency (Δf) is inversely proportional to the length of the signal. Hence Δf is not the same for the shorter and longer time durations. However it was kept constant for a particular experiment during data processing. A Fourier transform converts a signal in the time domain to the frequency domain (spectrum).

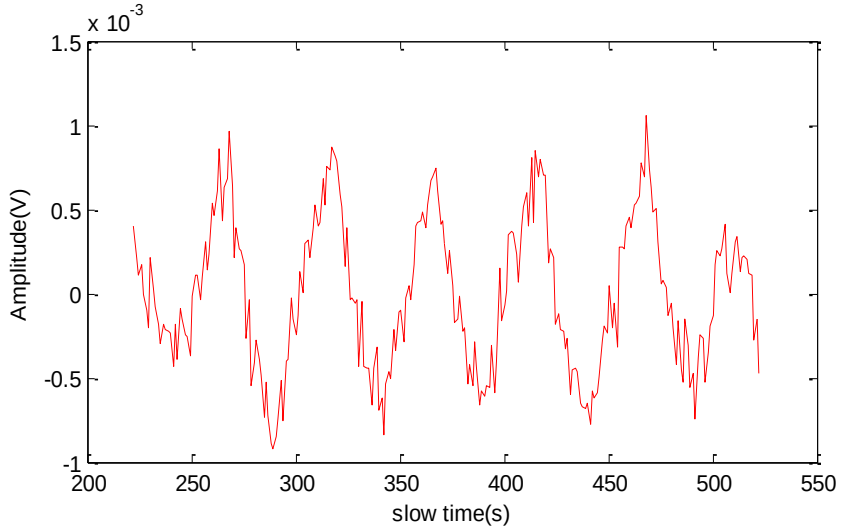

Figure 3.9: A part of a signal of a porcine heart window during electric field application.

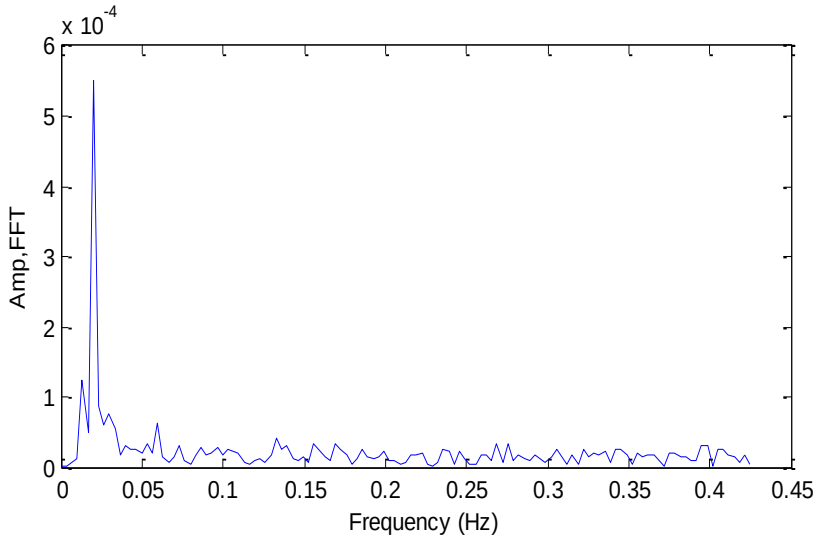

Figure 3.10 Frequency spectrum of the signal during current.

After the Fourier transformation of the signal during electric current, the amplitude of the frequency spectrum for each window in the sample was obtained corresponding to the frequency (0.02Hz) of the externally applied electric field. The amplitude of the frequency spectrum of various windows in the sample was compared at the particular frequency 0.02Hz (the frequency of the applied electric field). However, there are two disadvantages to use the amplitude at a single frequency of the spectrum to represent the EKP. The first one is that maximum peak might shift away from the selected frequency slightly as explained below. The second one is that the amplitude of the peak is proportional to the ultrasound signals amplitude, therefore dependent on the backscattering coefficient of the tissue or the impedance mismatch at interface. It is more desirable to have an EKP indicator that is independent of the backscattering coefficient of the tissue or the impedance mismatch. We will address these two issues by introducing the SNR analysis in the spectrum domain.

3.5.3 Observing the mean signal and root mean square value of the noise

The mean amplitude of the frequency spectrum at 0.02Hz was calculated and represented as the mean signal. The frequency spectrum of the windows in the whole sample during the electric field application was obtained to find the mean amplitude of the signal spectrum and the root mean square of the noise. Mean signal (A_{mean}) was calculated by taking the mean amplitude of 11 corresponding frequencies 5 at the left and 5 at the right of 0.02Hz for each window in the sample for longer time experiments using porcine heart muscle and gelatin sample. On the other hand, the mean signal was calculated by taking the mean amplitude of 7 corresponding frequencies 3 at the left and 3 at the right of 0.02Hz because we applied at most tens of cycles of sinusoidal waves. The peak frequency in the spectrum can shift back and forth slightly different for longer and shorter time durations as explained in the section 3.5.2. In addition, we also want to consider the frequency components other than the maximum point. Essentially we are calculating the area under the peak. The 5 corresponding points at the left and right of the 0.02Hz for longer time experiment and 3 corresponding points at the left and right of the 0.02Hz for shorter time experiment was enough to get the mean amplitude at the maximum peak because it covers all the frequency components slightly below and above the 0.02Hz. The mean signal for longer time duration was calculated by using the equation (3.1) and the code was developed in the Matlab for longer and shorter time durations respectively

$$A_{mean} = \frac{\sum_{i=-5}^{5} A_i}{11} \qquad (3.1)$$

Where, A_i is the amplitude corresponding to i^{th} frequency in the spectrum and i is an integer.

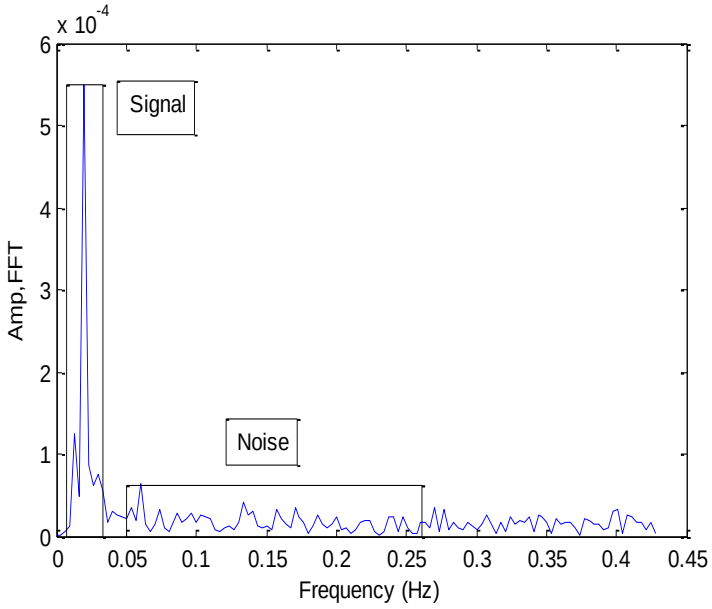

Figure 3.11: Schematic representation of signal and noise in the spectrum

Noise is measured as a statistical variable so it is quantified by its root mean square (RMS) value. The part of the amplitude of the spectrum between the frequencies 0.05Hz and the 0.25Hz is considered as the noise in the signal as shown in the Fig (3.11) and the code was developed in Matlab. Since there are many small peak amplitudes and any one is not representative of the noise over all. Amplitudes of the frequencies between 0.05Hz to 0.25Hz were squared and then took the square root of the mean value. The resultant measure is referred to as the root-mean-square or RMS amplitude (A_{rms}) of the noise which is given by the equation (3.2) [50], [51],[52]

$$A_{rms} = \sqrt{\frac{1}{N} \sum [A(n)]^2} \qquad (3.2)$$

Where N is the total number of points (frequencies) between 0.05Hz and 0.25Hz, A is the amplitude of each small peaks corresponding to n^{th} frequencies in the spectrum. The mean signal and the noise in the frequency spectrum are shown in the Fig. (3.11).

3.5.4 Analyzing fluctuations in signal-to-noise ratio (SNR)

The ratio of the mean signal at 0.02Hz to the root mean square of the noise for all the windows in the whole sample during electric field application was obtained and this ratio represents the signal-to-noise ratio (SNR). We examined the signal-to-noise ratio characteristics in a variety of tissues (porcine heart muscle, porcine fat) and gelatin phantoms to monitor the mechanical changes due to physiological level electric field application. The formula used to find the SNR is shown in equation (3.3) and the algorithm was developed in Matlab.

$$\text{Signal-to-noise ratio (SNR)} = \frac{Mean\ signal}{RMS\ noise} = \frac{A_{mean}}{A_{rms}} \qquad (3.3)$$

The mean signal and the RMS noise can be determined by using the algorithms developed in the Matlab on the basis of equation (3.1) and (3.2). In this study, the signal-to-noise ratio (SNR) in longer time experiment (samples separated by the thin plastic and without separated) as well as for shorter time experiment (samples not separated by the thin plastic) for the whole sample was compared in order to characterize the tissues and phantoms based on electro-kinetic phenomena.

Chapter 4

Results

Organization of the chapter

The results obtained by processing the data from various experiments are analyzed and discussed in this chapter. To begin, the results are arranged in four different steps. In the first step, the ultrasound RF signal versus fast time with the front, middle and rear boundaries were presented. In the second step, the mean of the signal spectrum at the modulation frequency and the RMS noise results during electric field application were presented for all the tissues and samples. In the third step, the plots of signal-to-noise ratio were presented with fast time in order to characterize the tissues and samples and finally, amplitude change of the windows in the tissues and samples with slow time before, during and after the electric field application along with their frequency spectrums of the signals during electric field application were presented.

4.1 Shorter time experiment using porcine heart and gelatin sample

Experiment parameters:

Electric field : 8Vp-p, 0.02Hz, 1.33V/cm

Sample : Porcine heart (6cm × 4cm × 0.74cm) and gelatin (6cm × 4cm × 0.43cm) both separated by thin plastic.

Start of application: 191s

End of application : 572s

4.1.1 Presentation of the results (Ultrasound RF signal, mean of the signal, RMS noise and signal-to-noise ratio)

The electric field was applied on the porcine heart sample using the electrodes and the gelatin sample was separated by thin plastic during the acquisition of the data. The porcine heart sample was placed on the top of the gelatin sample during the application of the electric field. Fig. 4.1(a) shows the RF signal versus fast time which is related to the thickness of the sample in the Z-axis in terms of the travel time of the ultrasound echo from the sample. In this experiment, the two samples were separated by the thin plastic so that the current would not flow from porcine heart tissue to the gelatin sample. In the RF echo signal, the fast time 17.37μs, 27.2μs and 32.9μs correspond to the front boundary of the porcine heart tissue, the boundary between porcine heart and the gelatin and the rear boundary of the gelatin sample. Mean signal, RMS of the noise and signal-to-noise ratios (SNR) with fast time are shown in the Fig. 4.1 (b) and (c) and (d). The dark lines at the fast time 27.2 μs in the Fig (b), (c) and (d) indicate the boundary of porcine heart and the gelatin sample.

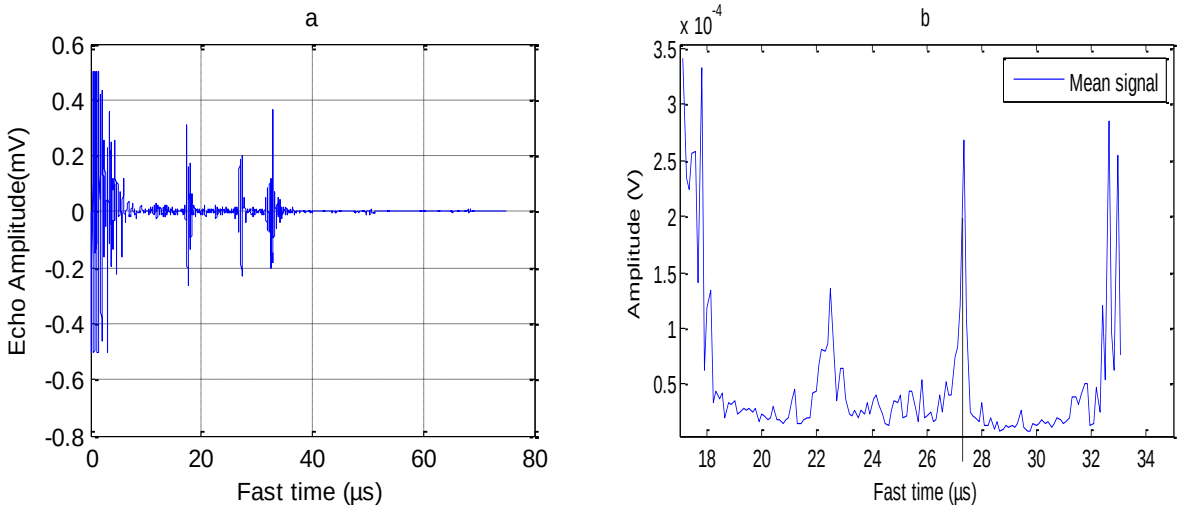

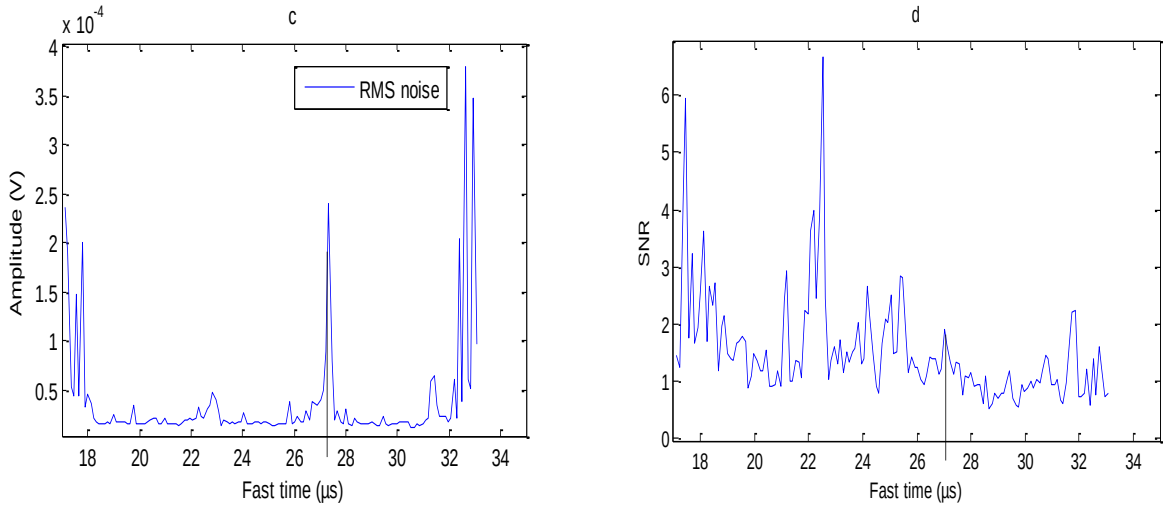

Figure 4.1: (a) Ultrasound RF signal versus fast time. (b) Mean of the signal. (c) Root mean square (RMS) of the noise. (d) Signal-to-noise ratio with fast time.

4.1.2 Amplitude versus slow time and their spectra during the application of electric field

During the application of the electric field the amplitude of the porcine heart windows changes continuously at the same frequency as the applied voltage as shown in the Fig. 4.2 (a), (c) and (e). Amplitude change is not same for all the windows of the porcine heart sample and they have different characteristics to electric field application as shown in the Fig 4.2 (g) and (h). Amplitude change increases in some windows and decreases in others. Amplitude changes of some windows in the gelatin sample are shown in the Fig. 4.2 (i), and (k). The gelatin sample has no electric field application and it was separated from the porcine heart sample by using a thin plastic. The small oscillation at some time is due to the experimental conditions**.** The frequency spectrums of the gelatin windows are shown in Fig. 4.2 (j) and (l).

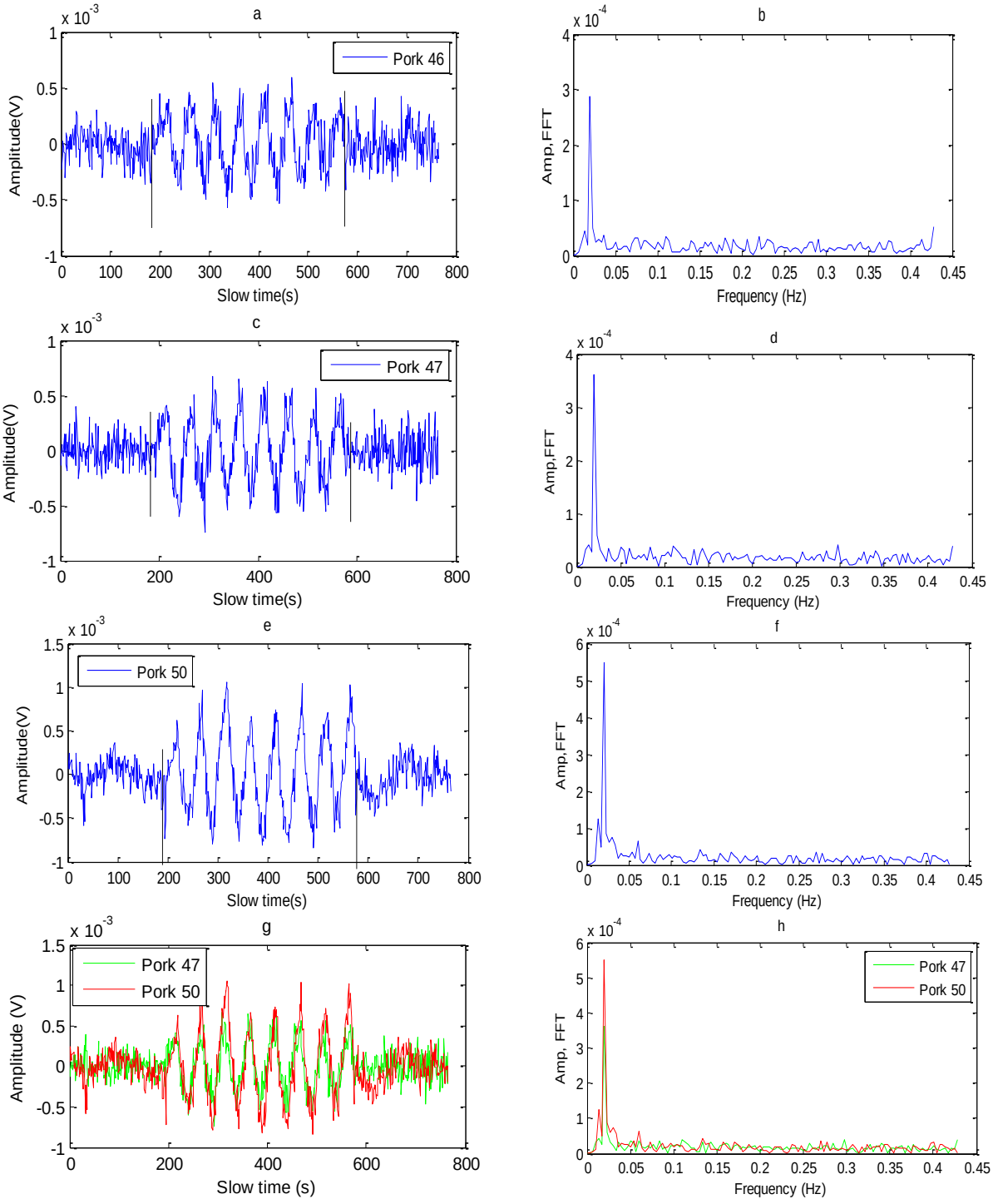
a
x 10^-3
Pork 46
Amplitude(V)
Slow time(s)
b
x 10^-4
Amp.FFT
Frequency (Hz)
c
x 10^-3
Pork 47
Amplitude(V)
Slow time(s)
d
x 10^-4
Amp.FFT
Frequency (Hz)
e
x 10^-3
Pork 50
Amplitude(V)
Slow time(s)
f
x 10^-4
Amp.FFT
Frequency (Hz)
g
x 10^-3
Pork 47
Pork 50
Amplitude (V)
Slow time (s)
h
x 10^-4
Pork 47
Pork 50
Amp, FFT
Frequency (Hz)

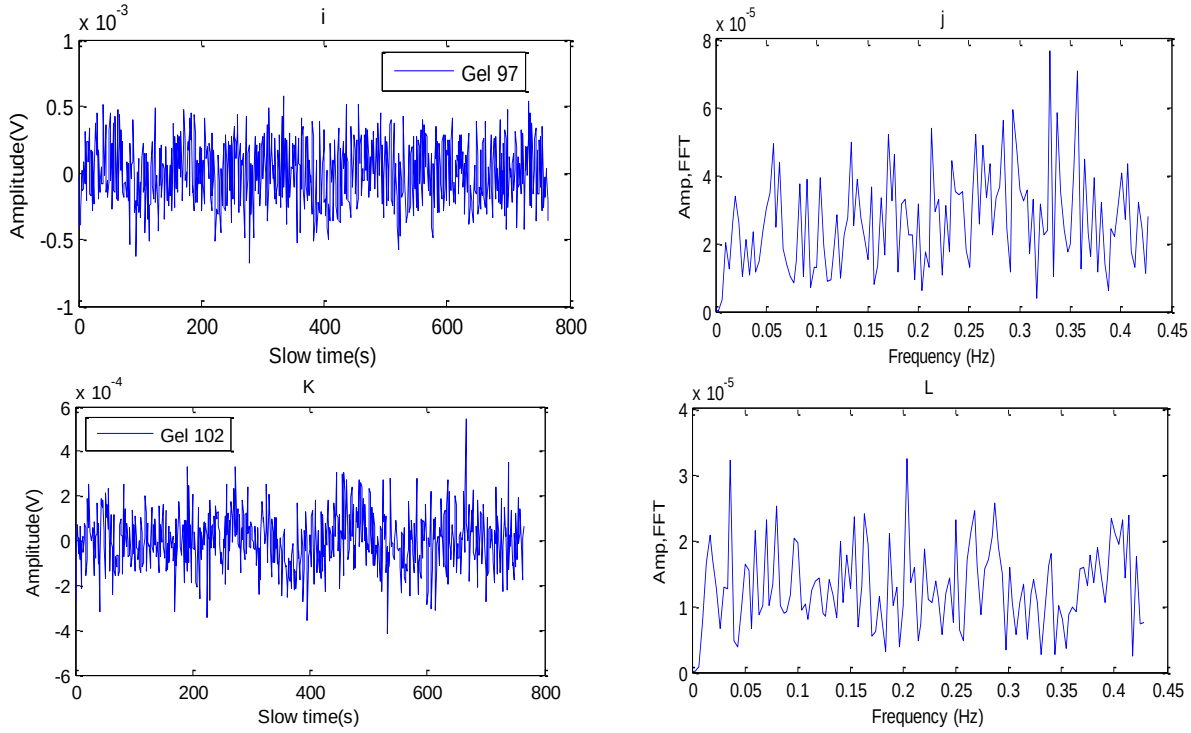

Figure 4.2: (a), (c) and (e) are amplitude changes of porcine heart windows 46, 47 and 50. (b), (d) and (f) are frequency spectrums during electric current of porcine heart windows 46, 47 and 50 respectively. (g) and (h) are comparison of the amplitude changes of porcine heart windows 47 and 50 respectively. (i), (k) and (j), (l) are the amplitude changes and frequency spectrums of the gelatin windows 97 and 102 respectively

4.2 Longer time experiment using porcine heart muscle and gelatin sample

Experiment parameters:

Electric field : 8Vp-p, 0.02Hz, 1.33V/cm

Sample : porcine heart (6cm × 4cm × 0.75cm) and Gelatin sample (6cm × 4cm × 0.55cm) both separated by thin plastic.

Start of application : 209s

End of application : 1223s

4.2.1 Presentation of the results (Ultrasound RF signal, mean of the signal, RMS noise and signal-to-noise ratio)

The electric field was applied on the porcine heart sample for 1014s by using the electrodes and the gelatin sample was separated by thin plastic during the experiment. The porcine heart sample was placed on the top of the gelatin sample during the application of the electric field. In this experiment, thin plastic was placed in between porcine heart and gelatin sample to stop the flow of current from porcine heart tissue to the gelatin sample during electric field application. In the RF echo signal, the fast time 20.29µs, 30.29µs and 37.73µs correspond to the front boundary of the porcine heart tissue, the boundary between porcine heart and gelatin and the rear boundary of the gelatin sample. Mean signal, RMS of the noise and signal-to-noise ratio (SNR) are shown in the Fig. 4.3 (b) and (c) and (d). The dark lines at the fast time 30.29 µs in the Fig (b), (c) and (d) indicate the boundary of porcine heart and the gelatin sample.

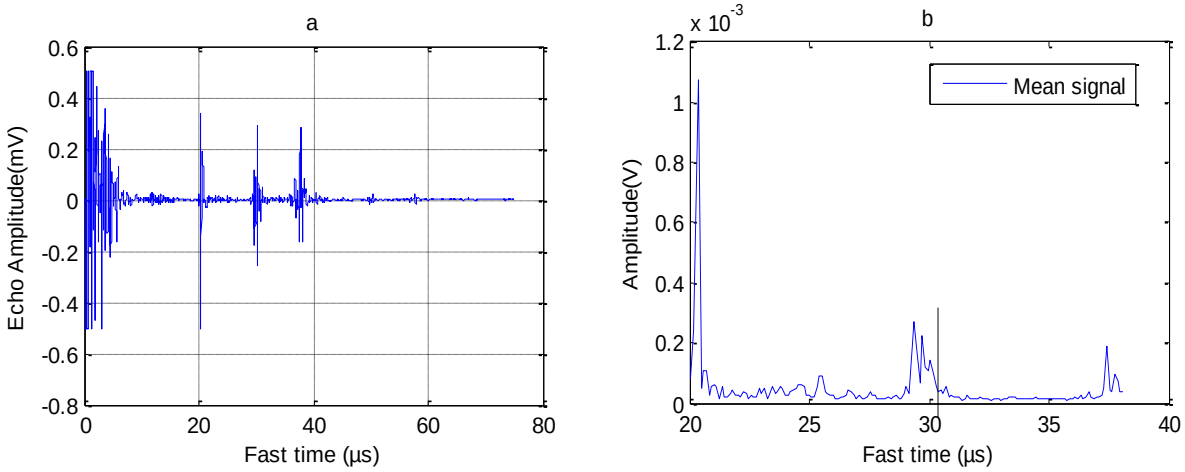

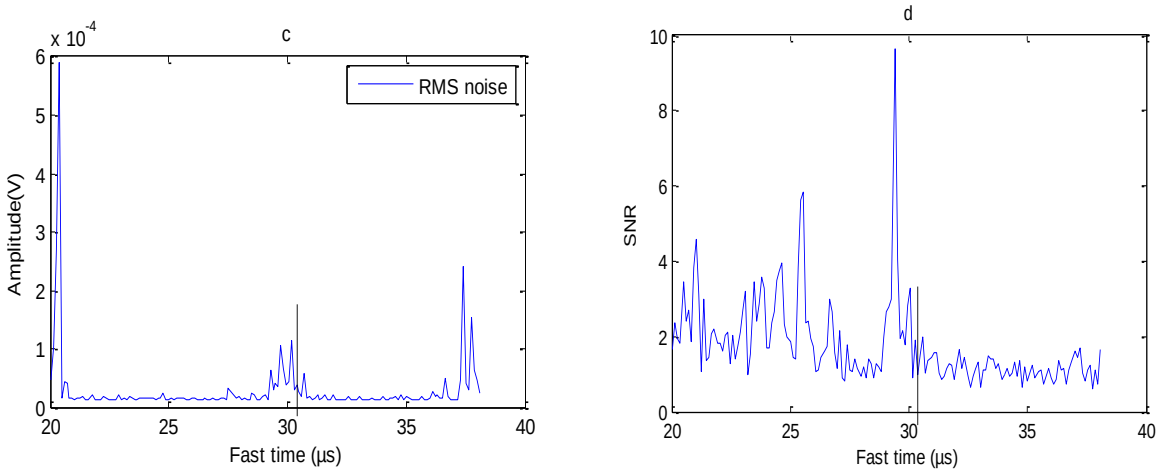

Figure 4.3: (a) Ultrasound RF signal versus fast time. (b) Mean of the signal. (c) Root mean square (RMS) of the noise. (d) Signal-to-noise ratio (SNR) with fast time.

4.2.2 Amplitude versus slow time and their spectra during the application of electric field

During the application of the electric field the amplitude of the porcine heart windows changes continuously at the same frequency (0.02Hz) as the applied voltage as shown in the Fig. 4.4 (a), (c) and (e). Amplitude change is not same for all the windows of the porcine heart sample and they have different characteristics to electric field application. Amplitude changes of some windows in the gelatin sample are shown in the Fig. 4.4 (g), and (i). The gelatin sample has no electric field application and it was separated from the porcine heart sample by using a thin plastic. The frequency spectrums of the gelatin windows are shown in Fig. 4.4 (h) and (j).

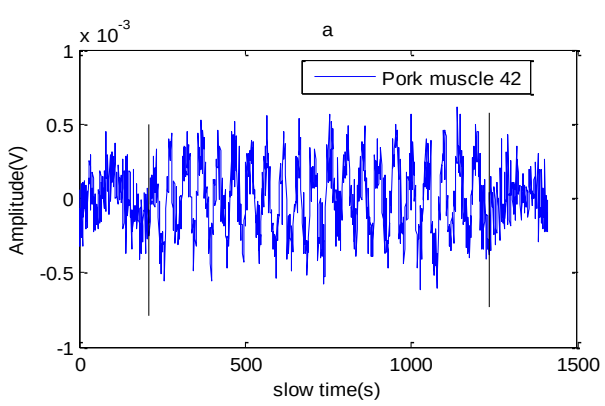
a
x 10^-3
Pork muscle 42
Amplitude(V)
slow time(s)

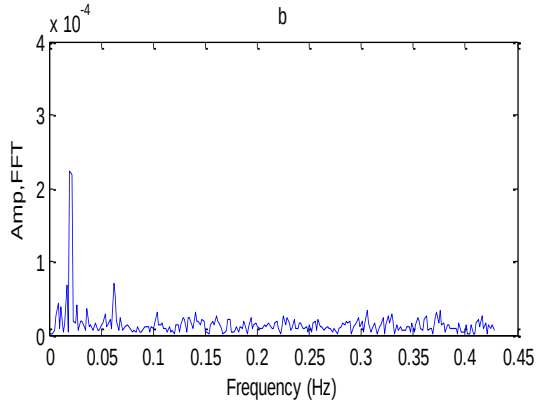
b
x 10^-4
Amp,FFT
Frequency (Hz)

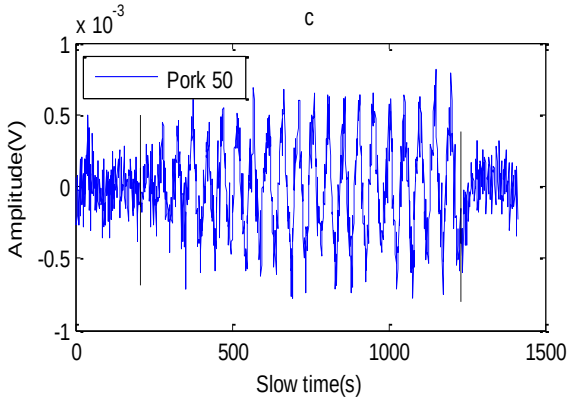
c
x 10^-3
Pork 50
Amplitude(V)
Slow time(s)

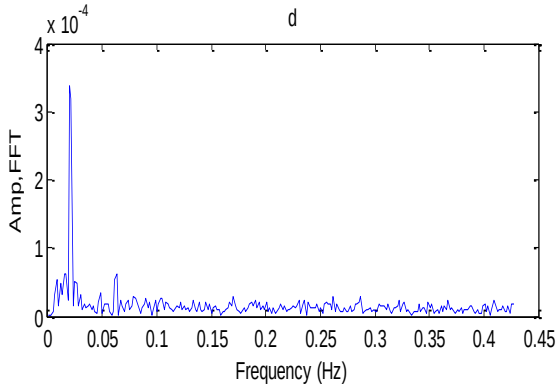
d
x 10^-4
Amp,FFT
Frequency (Hz)

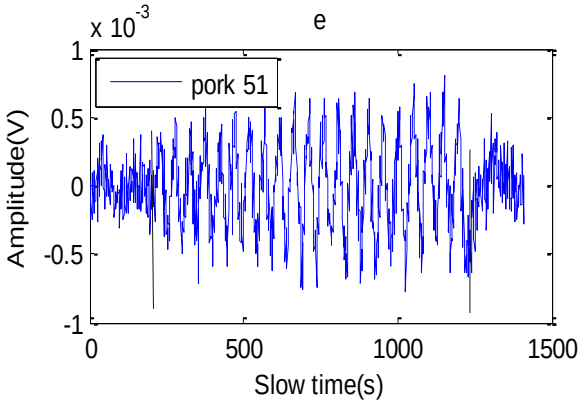
e
x 10^-3
pork 51
Amplitude(V)
Slow time(s)

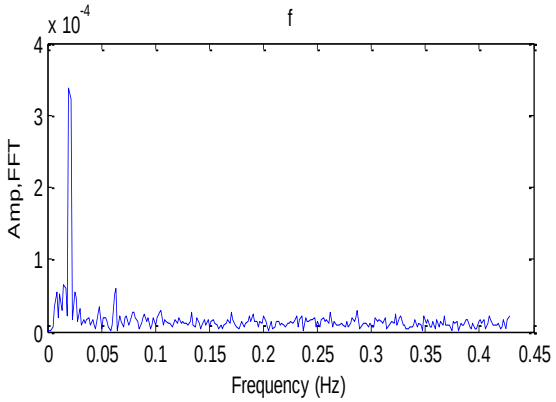
f
x 10^-4
Amp,FFT
Frequency (Hz)

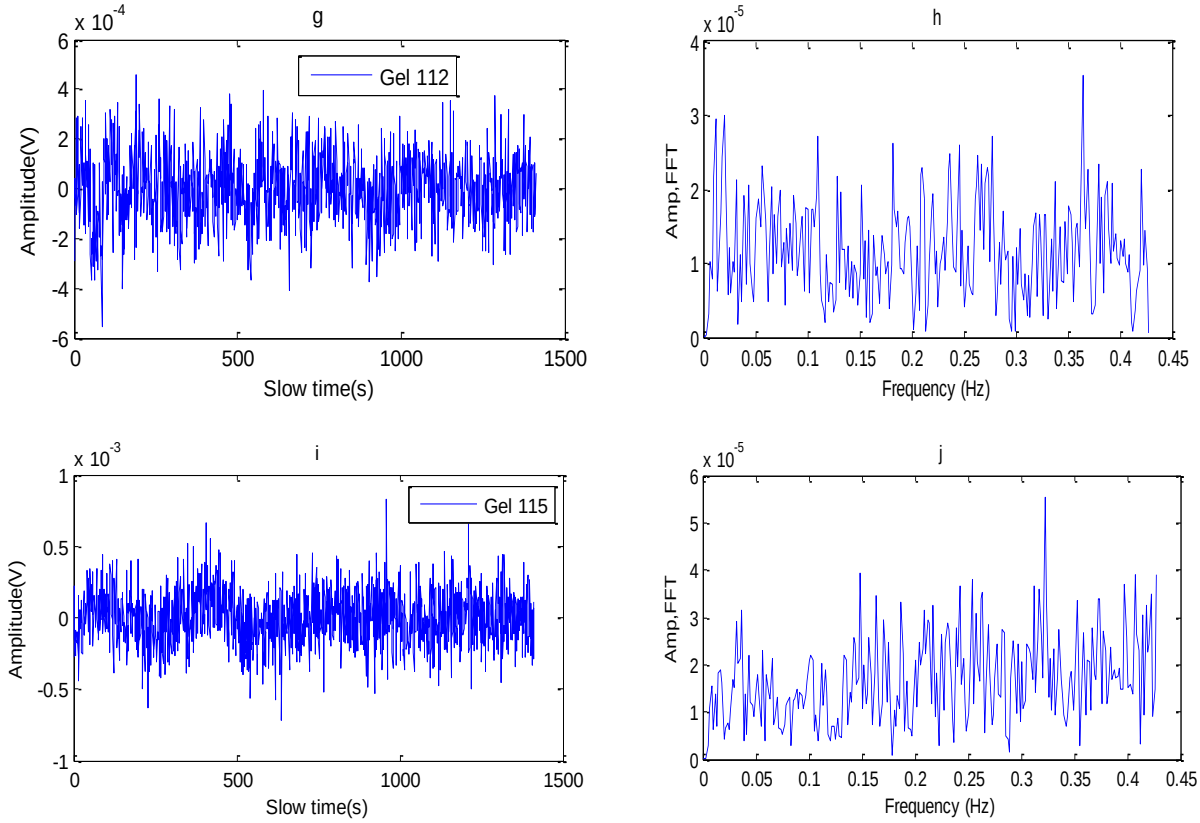

Figure 4.4: (a), (c) and (e) are amplitude changes of porcine heart windows 42, 50 and 51. (b), (d) and (f) are frequency spectrums during electric current of porcine heart windows 42, 50 and 51 respectively. (g) and (i) are amplitude changes of gelatin windows 112 and 115 respectively. (h) and (j) are the frequency spectrums of the gelatin windows 112 and 115 respectively.

4.3 Longer time experiment using porcine heart muscle and gelatin sample placed in contact

Experiment parameters:

Electric field : 8Vp-p, 0.02Hz, 1.33V/cm

Sample : porcine heart (6cm × 4cm × 0.531cm) and Gelatin sample (6cm × 4cm × 0.47cm). No plastic between porcine heart and gelatin sample.

Start of application : 184s

End of application : 1243s

4.3.1 Presentation of the results (Ultrasound RF signal, mean of the signal, RMS noise and signal-to-noise ratio)

In this experiment, the electric field was applied on the porcine heart tissue for 1059s by using the electrodes. The porcine heart sample was placed on the top of the gelatin sample during the application of the electric field. Both samples were kept in a good contact (no plastic was placed between the samples) so that the current might flow from porcine heart tissue to the gelatin sample during electric field application. In the RF echo signal, the fast time 19.45µs, 26.54µs and 32.79µs correspond to the front boundary of the porcine heart tissue, the boundary between porcine heart and gelatin and the rear boundary of the gelatin sample. Mean signal, RMS of the noise and signal-to-noise ratio (SNR) are shown in the Fig. 4.5 (b) and (c) and (d). The dark lines at the fast time 26.54 µs in the Fig (b), (c) and (d) indicate the boundary of porcine heart and the gelatin sample.

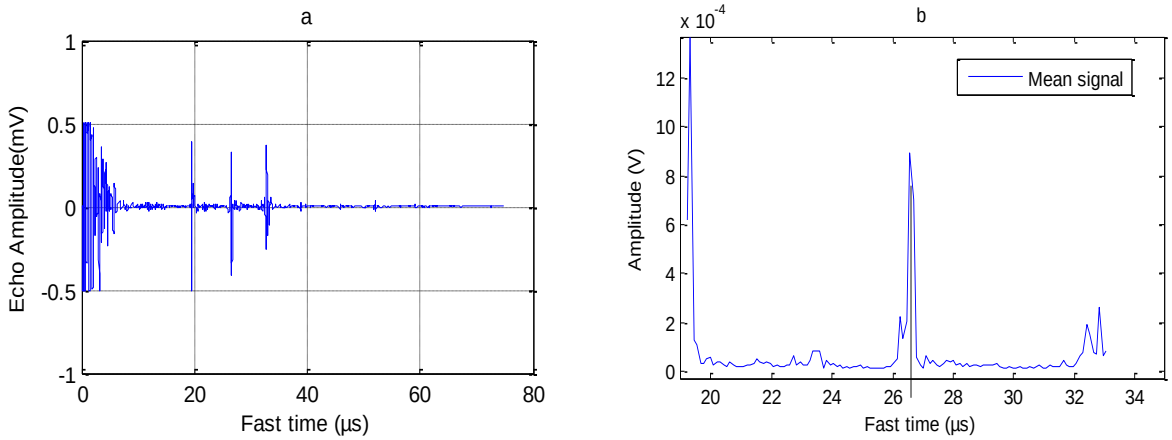

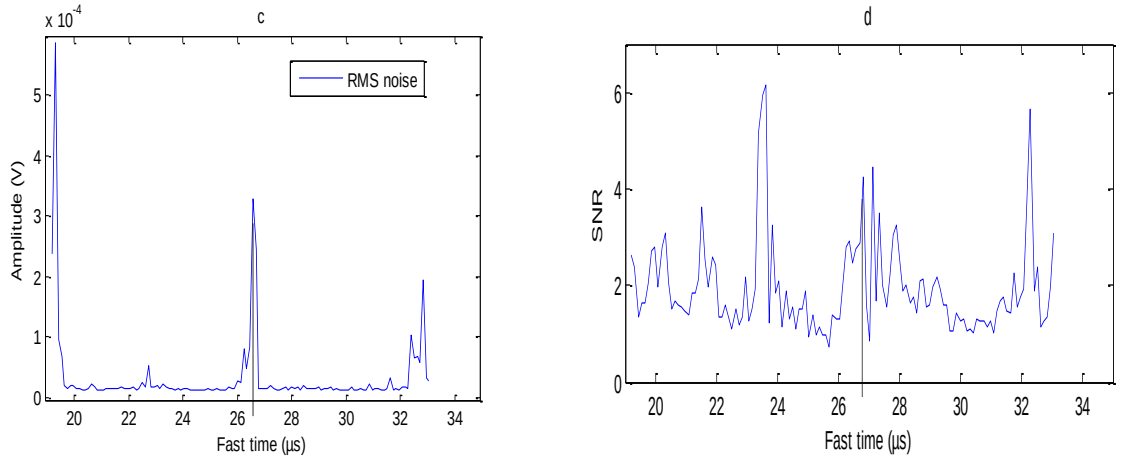

Figure 4.5: (a) Ultrasound RF signal versus fast time. (b) Mean of the signal. (c) Root mean square (RMS) of the noise. (d) Signal-to-noise ratio (SNR) with fast time.

4.3.2 Amplitude versus slow time and their spectra during the application of electric field

The gelatin sample was in good contact with the porcine heart sample during the experiment. The current flows from porcine heart sample to the gelatin during the electric field application and it induces some mechanical changes in the whole sample (porcine heart and gelatin). The amplitude of some gelatin windows changes continuously at the same frequency as the applied voltage however, the change in amplitude of the gelatin windows was found smaller than the porcine heart windows.

The amplitude change signal of some porcine heart windows before, during and after the electric field was stopped and gelatin windows are shown in the Fig (4.6). During the application of the electric field the amplitude of the porcine heart windows changes continuously at the same frequency (0.02Hz) as the applied voltage as shown in the Fig. 4.6 (a), (c) and (e). Amplitude changes of some windows in the gelatin sample with slow time are shown in the Fig. 4.6 (e), and (g) and their frequency spectrums are shown in the Fig. 4.6 (f) and (h).

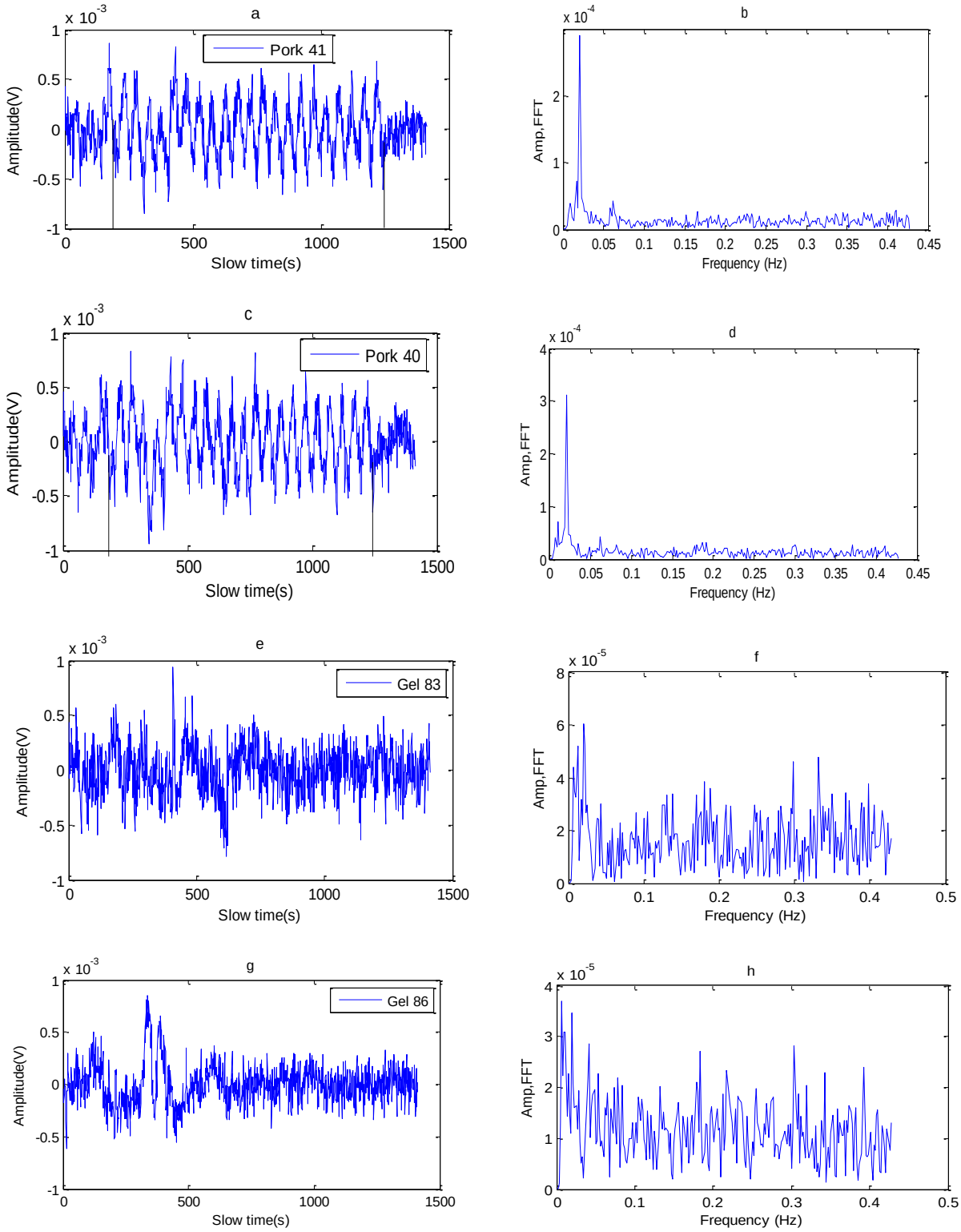

Figure 4.6: (a), (c) and (b), (d) are amplitude changes and frequency spectrum of porcine heart windows 41 and 40 respectively. (e), (g) and (f), (h) are the amplitude changes and frequency spectrums of gelatin windows 83 and 86 respectively.

4.4 Longer time experiment using layered tissues and phantoms (porcine heart, fat and gelatin sample)

Experiment parameters:

Electric field : 8Vp-p, 0.02Hz, 1.33V/cm

Sample : porcine heart at the top, porcine fat at the middle and gelatin at the bottom (no plastic between the samples).

Sample size : porcine heart (6cm × 4cm × 0.65cm), porcine fat (6cm × 4cm × 0.31cm) and gelatin (6cm ×4cm × 0.43cm)

Start of application : 217s

End of application : 1382s

4.4.1 Presentation of the results (Ultrasound RF signal, mean of the signal, RMS noise and signal-to-noise ratio)

This experiment was performed by using the porcine heart tissue, porcine fat and the gelatin sample. Electric field was applied on the porcine heart tissue for 1165s by using the electrodes. The porcine heart sample was placed on the top of the porcine fat and gelatin was placed at the bottom during the experiment. All the samples were kept in a good contact (no plastic was placed between the samples) with each other so that the current might flow from porcine heart tissue to the porcine fat and finally to the gelatin sample during electric field application.

In the RF echo signal, the fast time 18.51μs, 27.29μs, 31.38 μs and 37.31μs correspond to the front boundary of the porcine heart tissue, the boundary between porcine heart and fat, boundary between porcine fat and gelatin and the rear boundary of the gelatin sample. Mean signal, RMS of the noise and signal-to-noise ratio (SNR) are shown in the Fig. 4.7 (b) and (c)

and (d). The dark lines at the fast time 27.29µs and 31.38 µs in the Fig (b), (c) and (d) indicate the porcine-fat and the fat-gelatin boundary. The SNR in fat near the porcine heart muscle was found higher than the other parts of the fat as shown in the Fig. 4.7 (d).

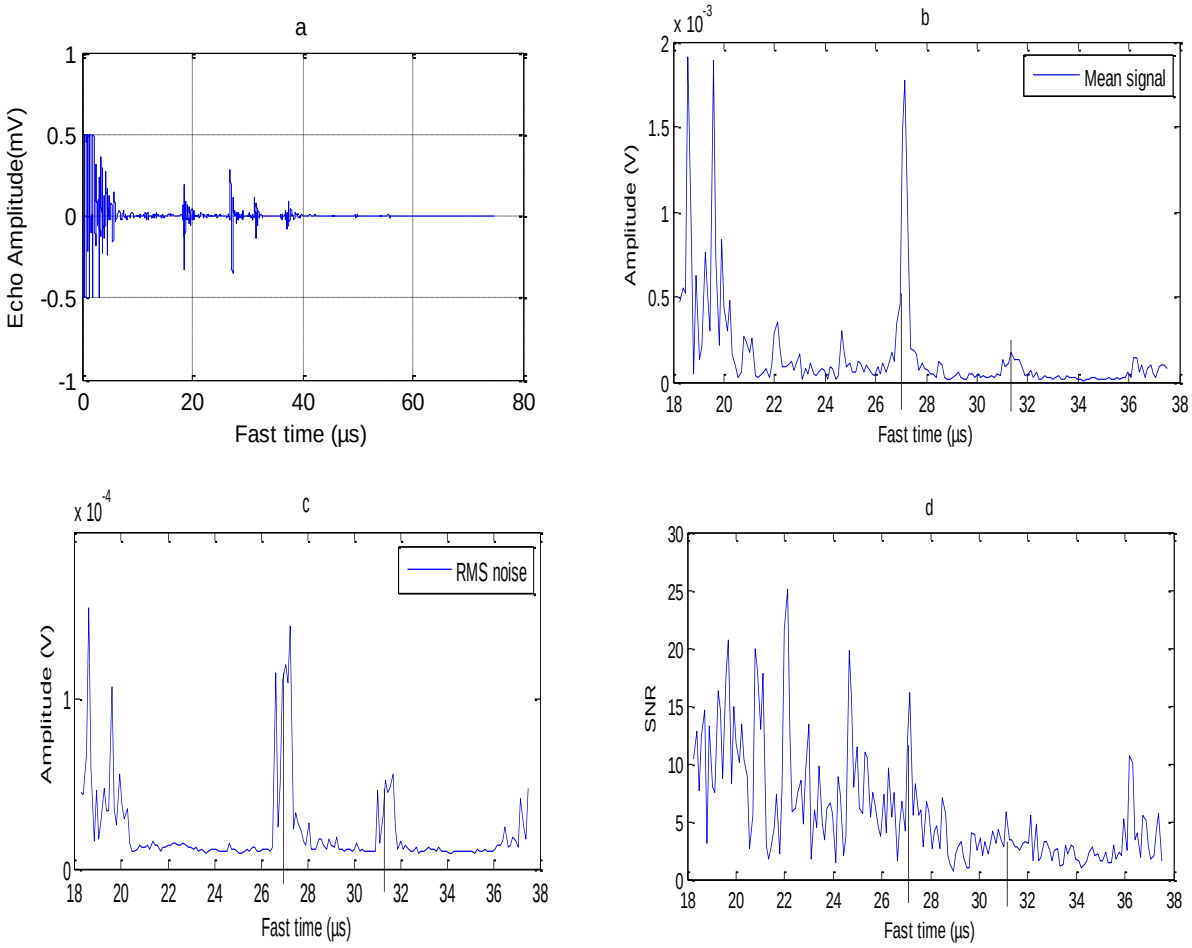

Figure 4.7: (a) Ultrasound RF signal versus fast time. (b) Mean of the signal. (c) Root mean square (RMS) of the noise. (d) Signal-to-noise ratio (SNR) with fast time.

4.4.2 Amplitude versus slow time and their spectra during the application of electric field

The current flows from porcine heart sample to the porcine fat and gelatin sample during electric field application. It induced some mechanical changes in the whole sample (porcine heart fat and gelatin). The amplitude of some fat and gelatin windows changes continuously at the same frequency as the applied voltage however, the change in amplitude of the fat and gelatin windows was not same during current.

The amplitude change signals of some porcine heart windows before, during the electric field and after the electric field was stopped are shown in the Fig (4.8). During the application of the electric field the amplitude of the porcine heart windows changes continuously at the same frequency (0.02Hz) as the applied voltage as shown in the Fig. 4.8 (a) and (c). Amplitude changes of some windows in fat and gelatin sample with slow time are shown in the Fig. 4.8 (e), (g) and (i), (k) respectively.

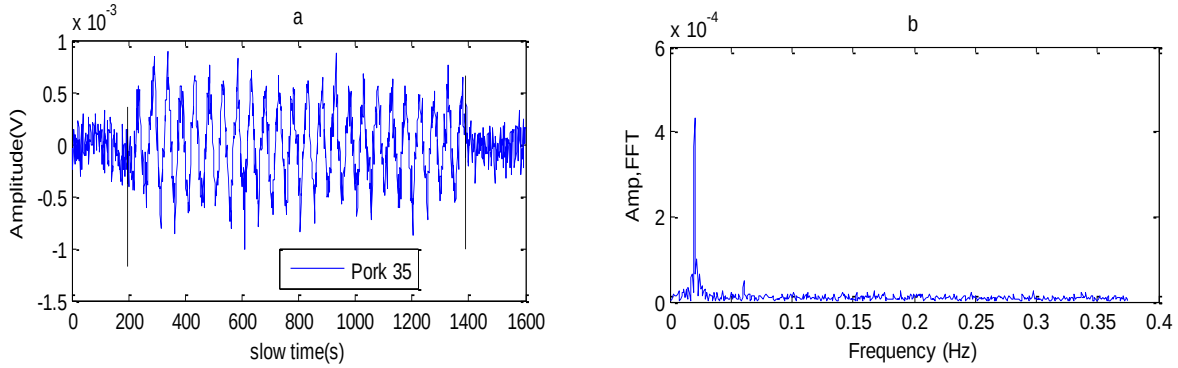

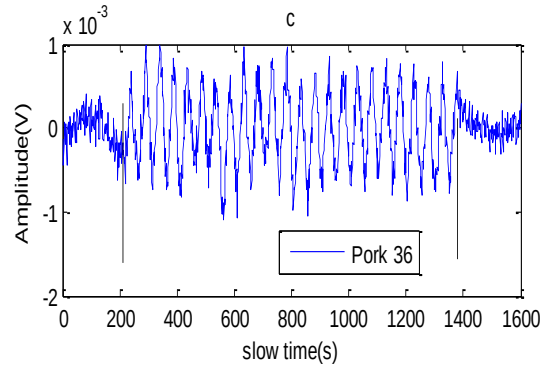
c
x 10^-3
Amplitude(V)
slow time(s)
Pork 36

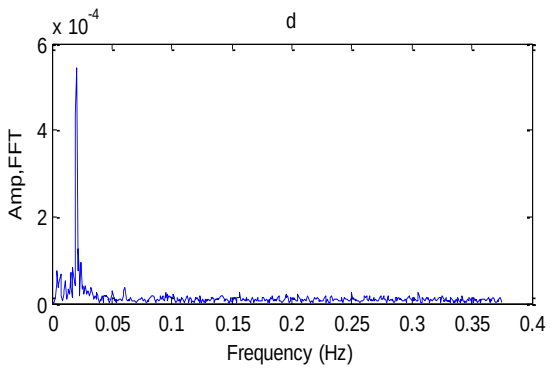
d
x 10^-4
Amp.FFT
Frequency (Hz)

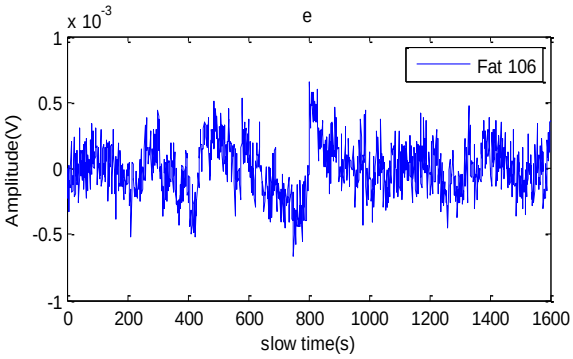
e
x 10^-3
Amplitude(V)
slow time(s)
Fat 106

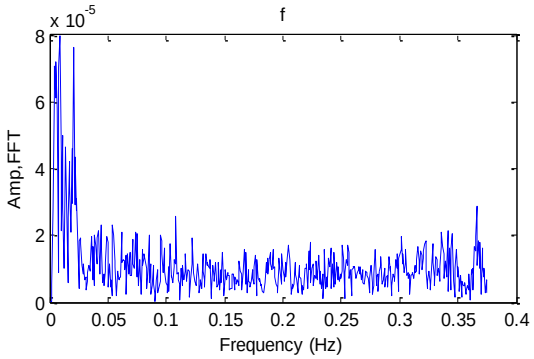
f
x 10^-5
Amp.FFT
Frequency (Hz)

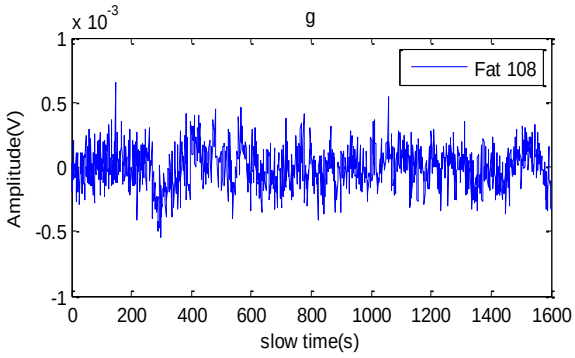
g
x 10^-3
Amplitude(V)
slow time(s)
Fat 108

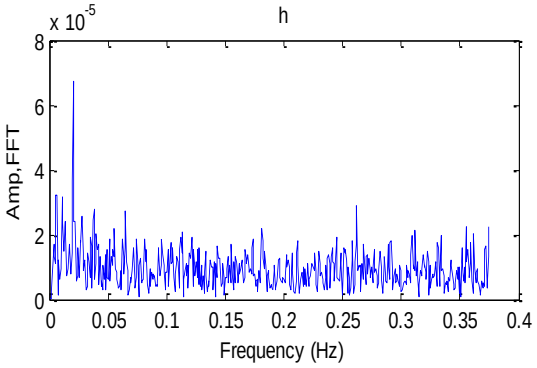
h
x 10^-5
Amp.FFT
Frequency (Hz)

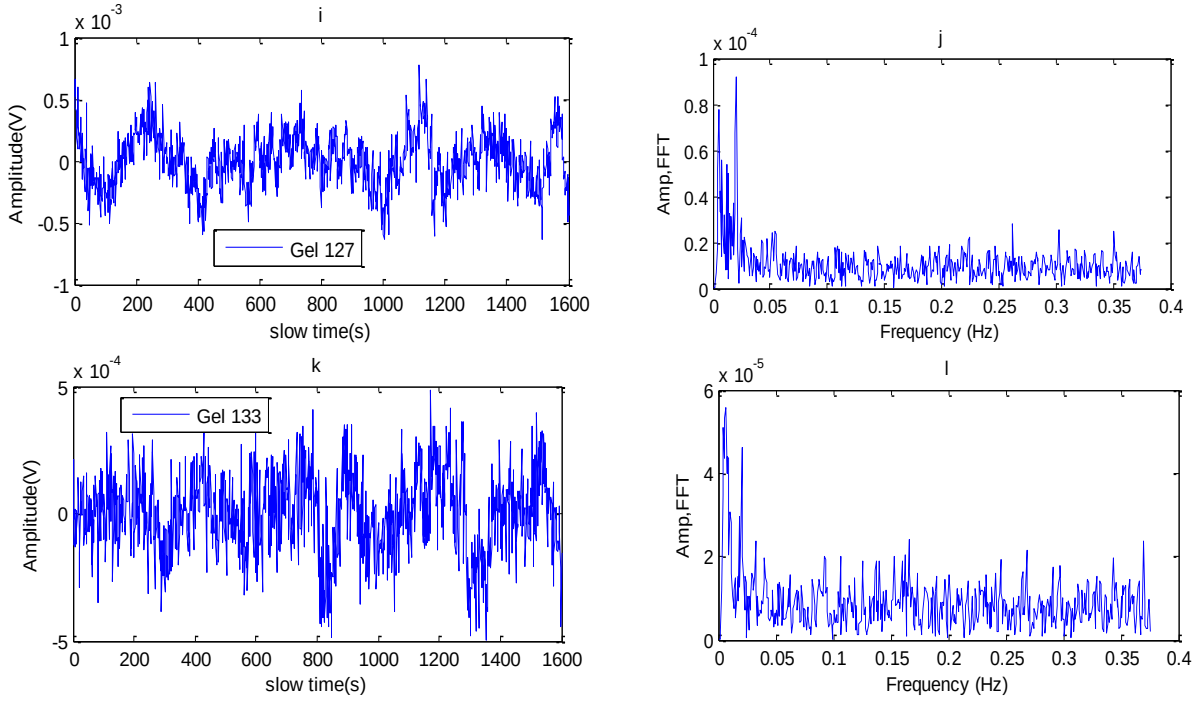

Figure 4.8: (a), (c) and (b), (d) are amplitude changes and frequency spectrums of porcine heart windows 35 and 36 respectively. (e), (g) and (f), (h) are the amplitude changes and frequency spectrums of fat windows 106 and 108 respectively. (i), (k) and (j), (l) are the amplitude changes and frequency spectrums of gelatin windows 127 and 133 respectively.

4.5 Longer time experiment using layered tissues and phantoms (porcine heart, fat and gelatin sample)

Experiment parameters:

Electric field : 8Vp-p, 0.02Hz, 1.33V/cm

Sample : porcine heart at the top, porcine fat at the middle and gelatin at the bottom (no plastic between the samples).

Sample size : porcine heart (6cm × 4cm × 0.48cm), porcine fat (6cm × 4cm × 0.46 cm) and gelatin (6cm ×4cm × 0.43cm)

Start of application : 182s

End of application : 1198s

4.5.1 Presentation of the results (Ultrasound RF signal, mean of the signal, RMS noise and signal-to-noise ratio)

Electric field was applied on the porcine heart tissue for 1016s by using the electrodes. Samples were kept in a good contact (no plastic was placed between the samples) with each other so that the current might flow from porcine heart tissue to the porcine fat and gelatin sample during electric field application.

In the RF echo signal, the fast time 19.41μs, 25.91μs, 32.11μs and 37.88μs correspond to the front boundary of the porcine heart tissue, porcine-fat boundary, fat- gelatin boundary and the rear boundary of the gelatin sample. Mean signal, RMS of the noise and signal-to-noise ratio (SNR) are shown in the Fig. 4.9 (b) and (c) and (d). The dark lines at the fast time 25.91μs and 32.11μs in the Fig (b), (c) and (d) indicate the porcine-fat and the fat-gelatin boundary.

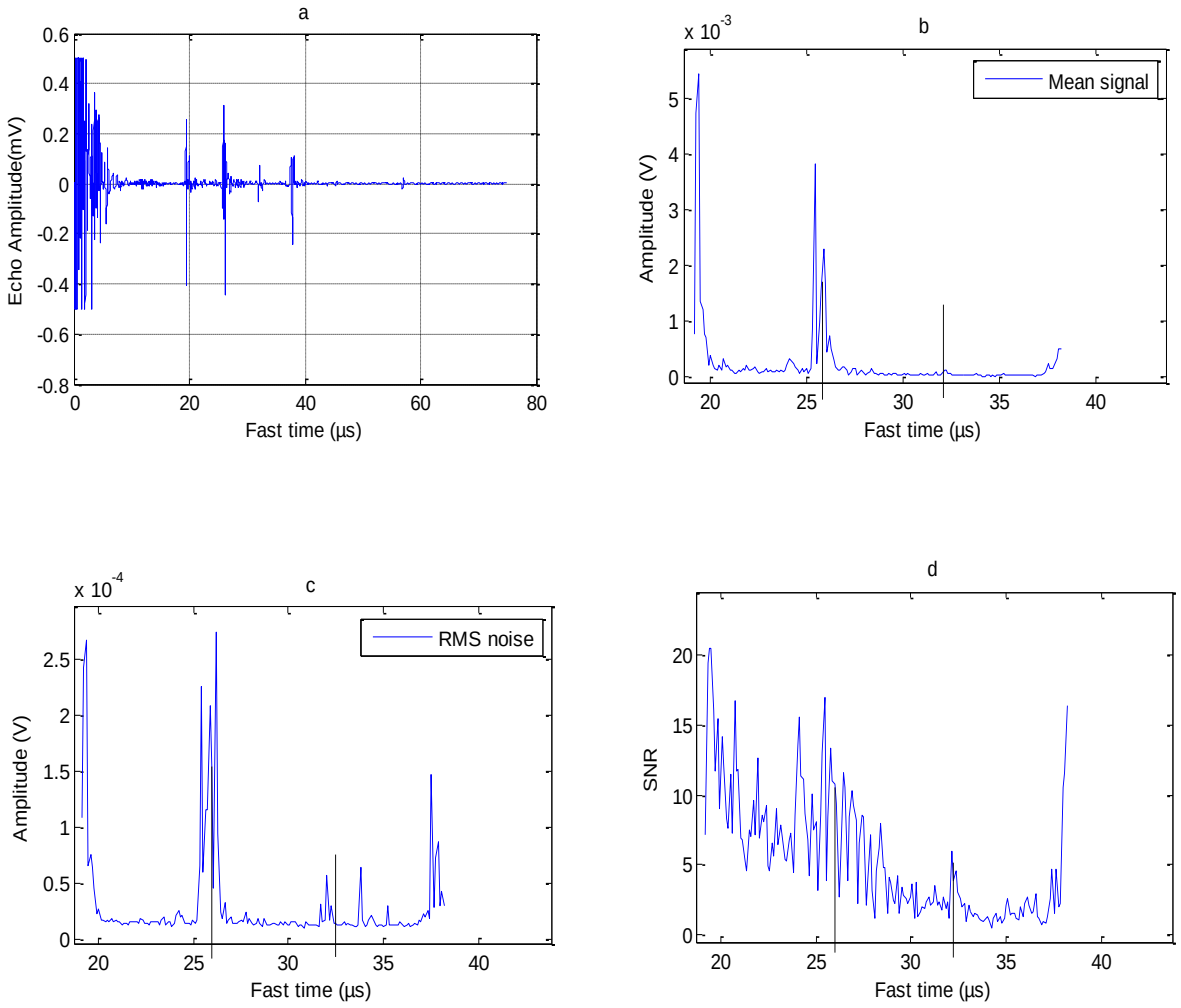

Figure 4.9: (a) Ultrasound RF signal versus fast time. (b) Mean of the signal. (c) Root mean square (RMS) of the noise. (d) Signal-to-noise ratio (SNR) with fast time.

4.5.2 Amplitude versus slow time and their spectra during the application of electric field

During the application of the electric field the amplitude of the porcine heart windows changes continuously at the same frequency (0.02Hz) as the applied voltage as shown in the Fig. 4.10 (a), and (c). Amplitude changes of some windows in fat and gelatin sample with slow time are shown in the Fig. 4.10 (e), (g) and (i), (k) respectively.

The current flows from porcine heart muscle to fat and gelatin sample during electric field application. It induced mechanical changes in the whole sample (porcine heart fat and gelatin). The amplitude of some fat and gelatin windows changes continuously at the same frequency as the applied voltage however, the change in amplitude of the fat and gelatin windows was not same during current.

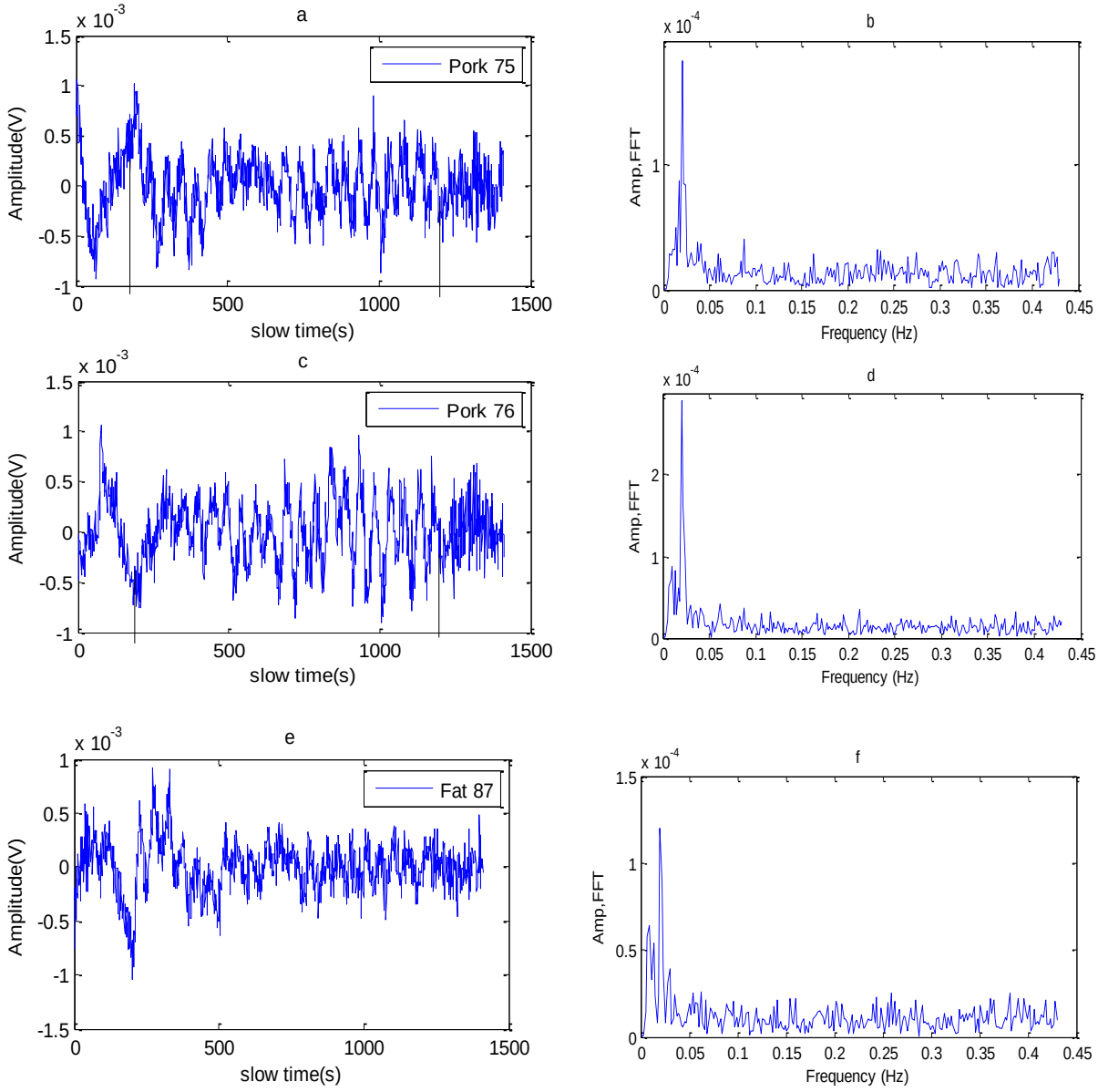

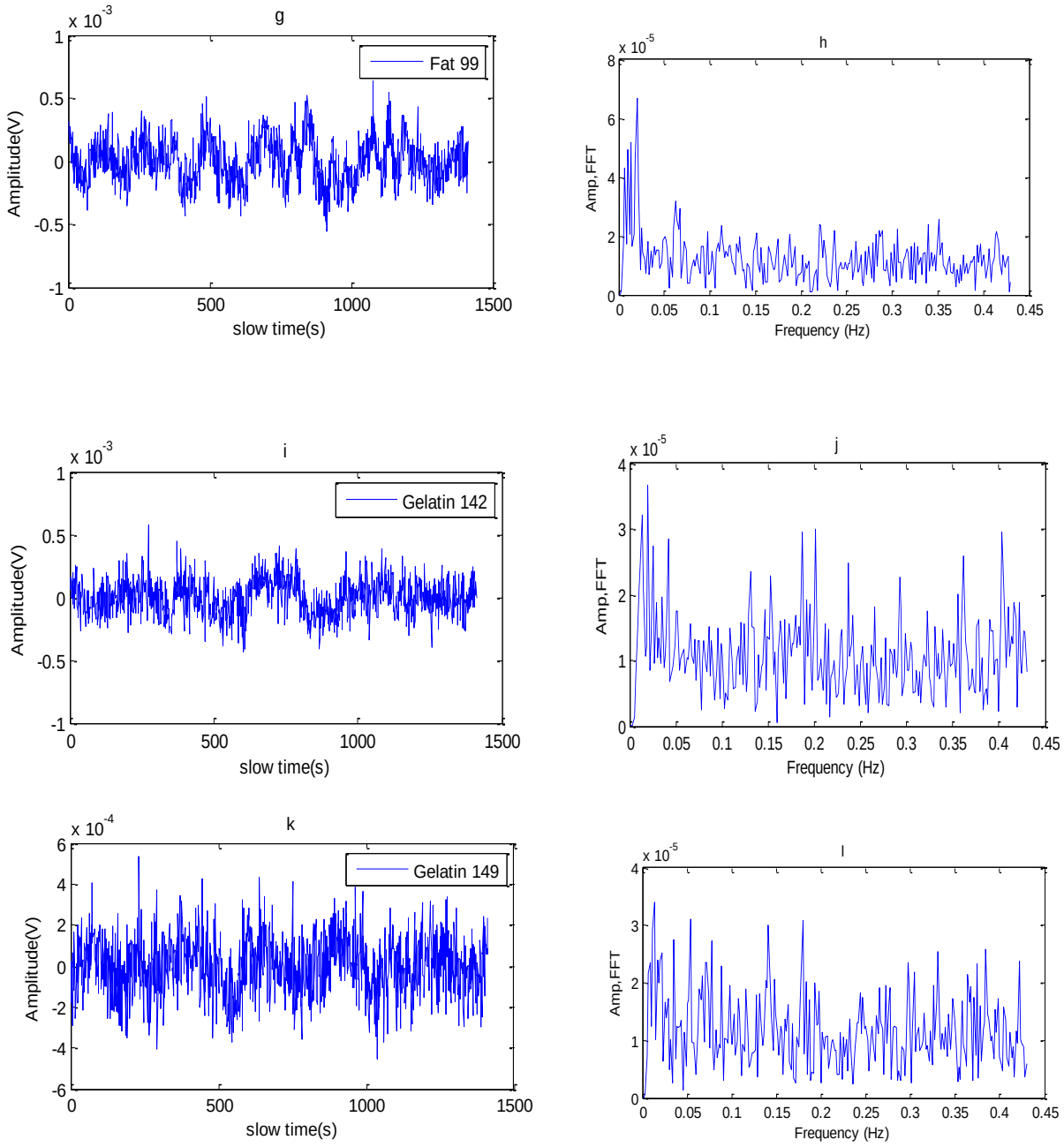

Figure 4.10: (a), (c) and (b), (d) are the amplitude changes and frequency spectrums of porcine heart windows 75 and 76 respectively. (e), (g) and (f), (h) are the amplitude changes and frequency spectrums of fat windows 87 and 99 respectively. (i), (k) and (j), (l) are the amplitude changes and frequency spectrums of gelatin windows 142 and 149 respectively.

4.6 Single gelatin experiment

Experiment parameters:

Electric field : 8Vp-p, 0.02Hz, 1.33V/cm

Sample size : gelatin (6cm ×4cm × 0.65cm)

Start of application : 191s

End of application : 1251s

4.6.1 Presentation of the results (Ultrasound RF signal, mean of the signal, RMS noise and signal-to-noise ratio)

In the previous experiments, we found that the EIMC SNR was not uniform for tissue samples that appeared uniform. To investigate if the source of this spatial heterogeneity of SNR, experiment was performed only using a uniform gelatin sample. Electric field was applied on the gelatin sample for 1060s by using the electrodes. In the RF echo signal, the fast time 20.41μs, and 29.02μs correspond to the front boundary and the rear boundary of the gelatin sample. Mean signal, RMS of the noise and signal-to-noise ratio (SNR) are shown in the Fig. 4.11 (b), (c) and (d). The dark lines at the fast time 20.41μs and 29.02μs in the Fig (b) and (c) indicates the front and rear boundary of the gelatin sample.

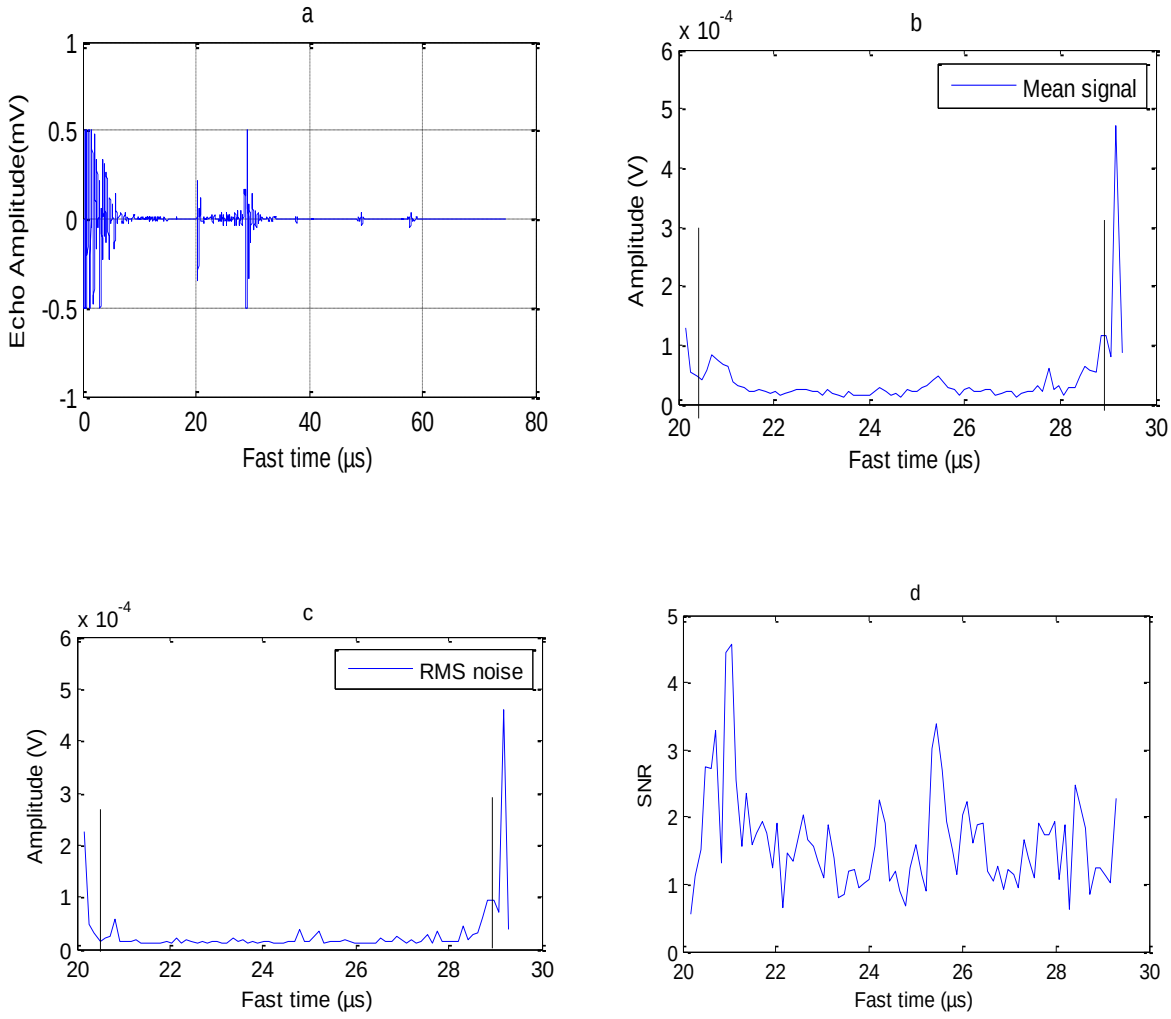

Figure 4.11: (a) Ultrasound RF signal versus fast time. (b) Mean of the signal. (c) Root mean square (RMS) of the noise. (d) Signal-to-noise ratio (SNR) with fast time.

4.6.2 Amplitude versus slow time and their spectra during the application of electric field

During the application of the electric field the amplitude of the gelatin windows changes continuously at the same frequency (0.02Hz) as the applied voltage as shown in the Fig. 4.12 (a), (c) and (e). The frequency spectrums are shown in the Fig 4.12 (b), (d) and (f) respectively. Electric field induced mechanical changes in the gelatin sample. The change in amplitude of the gelatin windows was not same during current.

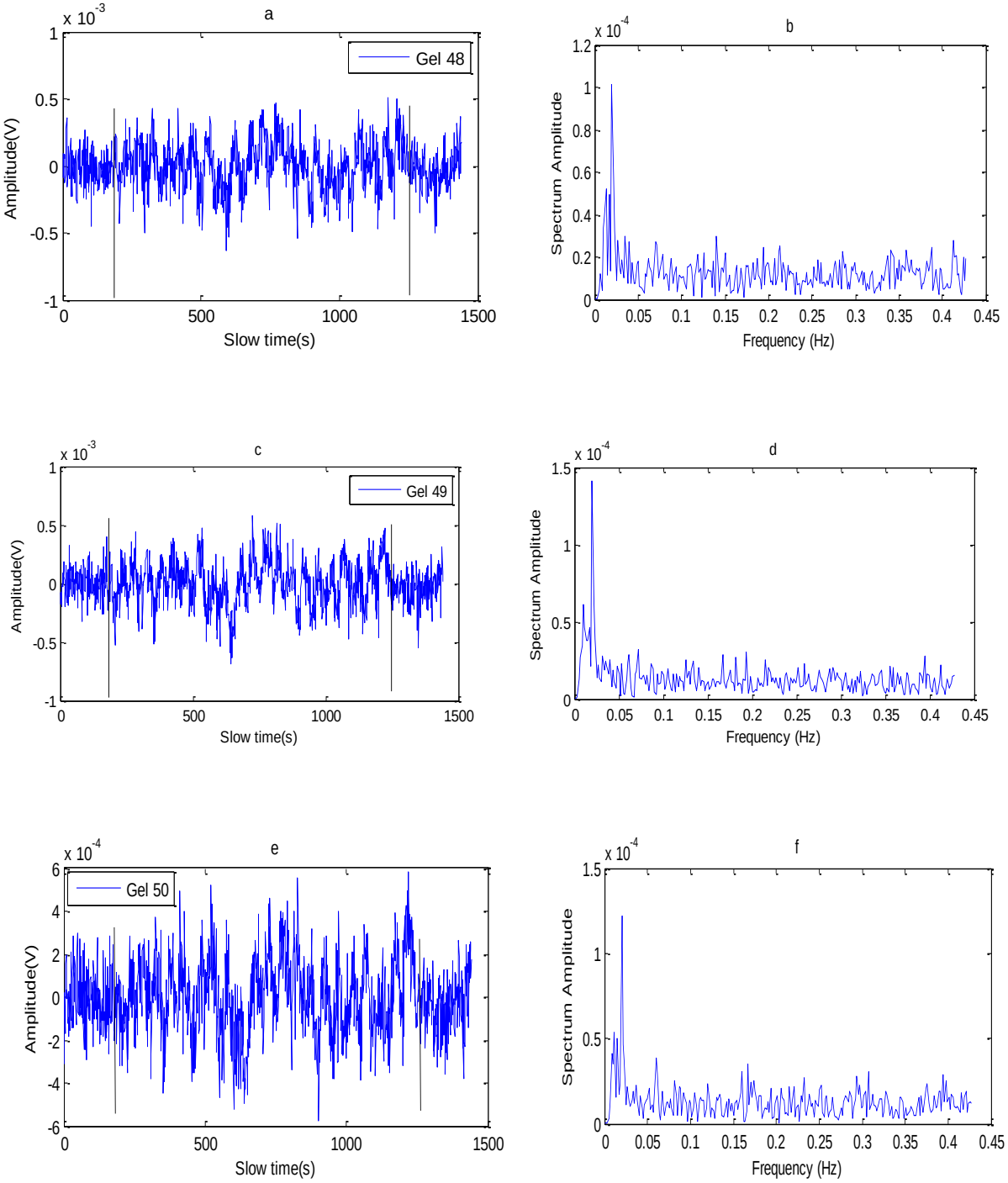

Figure 4.12: (a), (c) and (e) are the amplitude change signals of the gelatin windows and (b), (d), (f) are their spectrums respectively.

4.7 Longer time experiment using gelatin sample and porcine heart muscle

Experiment parameters:

Electric field : 8Vp-p, 0.02Hz, 1.33V/cm

Sample : gelatin at the top and porcine heart muscle at the bottom (no plastic between the samples).

Sample size : gelatin (6cm × 4cm × 0.44cm) and porcine heart muscle (6cm × 4cm × 0.67 cm)

Start of application : 191.17s

End of application : 1258s

4.7.1 Presentation of the results (Ultrasound RF signal, mean of the signal, RMS noise and signal-to-noise ratio)

In this experiment, the gelatin sample was placed on the top of the porcine heart muscle. Electric field was applied on the gelatin sample for 1066s by using the electrodes. Plastic was not placed between the samples during the experiment so that the current might flow from gelatin sample to the porcine heart muscle during electric field application.

In the RF echo signal, the fast time 23.3μs, 29.23μs, and 38.27μs correspond to the front boundary of the gelatin sample, gelatin-muscle boundary and the rear boundary of the porcine heart muscle sample. Mean signal, RMS of the noise and signal-to-noise ratio (SNR) are shown in the Fig. 4.13 (b) and (c) and (d). The dark lines at the fast time 23.3μs, 29.23 μs and 38.27μs in the Fig (b), (c) and (d) indicate the front boundary of the gelatin, gelatin-muscle boundary and the rear boundary of the porcine heart muscle.

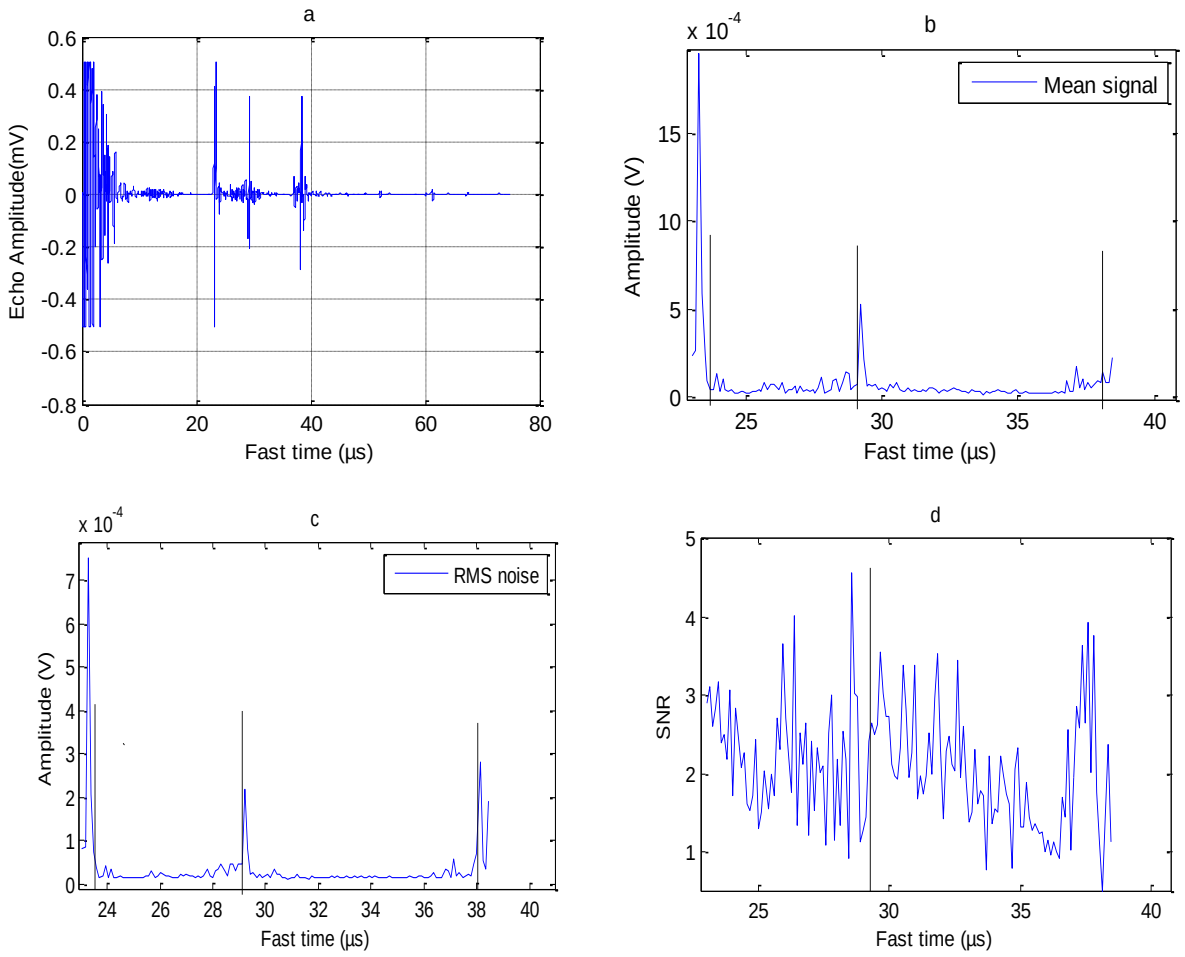

Figure 4.13: (a) Ultrasound RF signal versus fast time. (b) Mean of the signal. (c) Root mean square (RMS) of the noise. (d) Signal-to-noise ratio (SNR) with fast time.

4.7. 2 Amplitude versus slow time and their spectra during the application of electric field

The gelatin sample was placed on the top of the porcine heart muscle and both samples were in good contact with each other during the experiment. The current flows from gelatin sample to the porcine heart muscle during the electric field application which induced mechanical changes in the whole sample. The amplitude of gelatin and some muscle windows changes continuously at the same frequency as the applied voltage however, the change in amplitude was not same for all the windows.

Amplitude changes of some windows in the gelatin and muscle sample with slow time and their spectrums are shown in the Fig. 4.14.

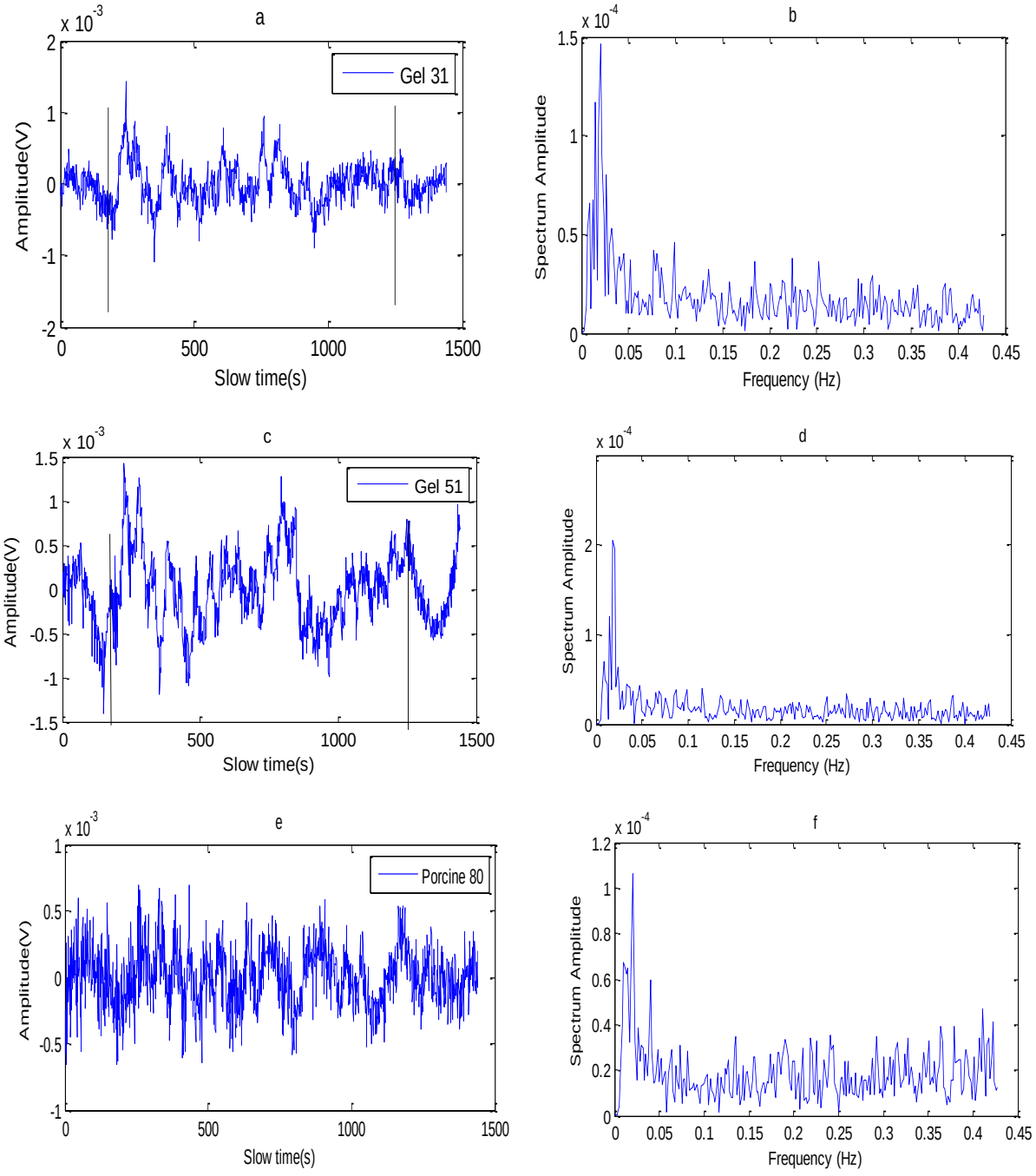

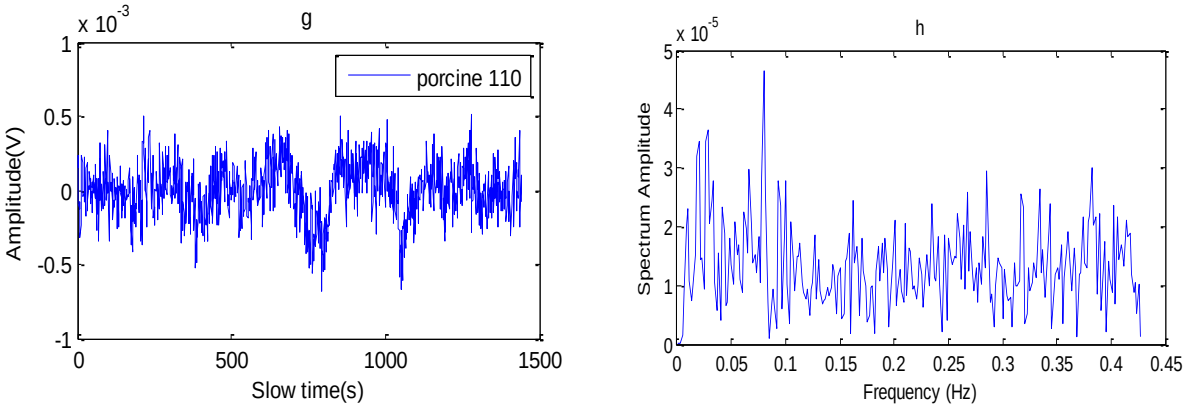

Figure 4.14: (a), (c) and (b), (d) are the amplitude change signals of the gelatin windows and their spectrums respectively. (e), (g) and (f), (h) are the amplitude change signals of the muscle windows and their spectrums respectively.

Chapter 5

Discussion and Conclusions

5.1 Discussion

Electro-kinetic effects have been used to explain the mechanical changes on layered tissues and gelatin phantoms when these are subject to an electric field. During the application of the electric field, the amplitude increases in some windows and decreases others. The amplitude changes continuously at the same frequency as the applied voltage (0.02Hz).

In order to study the characterization of tissues and phantom based on the amplitude change of ultrasound echo signal under the application of electric field, experiments were performed in two different ways by using porcine heart muscle, fat and the gelatin sample. Two experiments were performed only using the porcine heart muscle and the gelatin sample separated by the thin plastic (insulator). Electric field was applied on the porcine heart muscle for 381s and the 1014s represented by shorter time and the longer time experiments respectively, where gelatin was electrically isolated. The mean amplitude of the signal at frequency 0.02Hz for both longer and shorter time experiment indicate that the porcine heart muscle has more amplitude change than the gelatin sample. This is because there is no current in gelatin as there is an insulator between the tissue and the gelatin, where the current was applied. The RMS noise of the signals during current was almost the same for porcine heart and gelatin as shown in the Fig. 4.1 (c) and 4.3 (c). The spectra in Fig. 4.3 have less noise than those in Fig. 4.1 because the electric current was applied for a longer duration. The Fourier transform of a periodic signal with longer duration will

give better SNR in the spectra. It was found that almost 5 frequencies in the spectrums of the longer time experiment were under the same range of the 3 frequencies of the shorter time experiment.

In the section 4.1.1 and 4.2.1, experimental results were presented in which electric field was applied on the porcine heart muscle and the gelatin sample was separated by the plastic. The signal to noise ratio of the spectrum in the porcine sample was significantly larger than the gelatin sample. The larger SNR of the signals in the porcine heart sample agrees with the fact that electric current, and the induced mechanical changes in the porcine heart only exists in porcine tissue during electric field application .On the other hand, the SNR ≈1 in the gelatin sample because it has no electric field application which indicates that the signal change at 0.02 Hz in the gelatin sample is due to the random variation of the ultrasound signal amplitude. The random variation of the ultrasound signal amplitude has a broad spectrum.

However, in the porcine heart sample the SNR of the spectrum varies throughout the sample even though the sample looks homogeneous. Experiment was performed using a uniform gelatin sample and it was found that the SNR was not the same at all the locations and varies throughout the gelatin sample as shown in the Fig 4.11 (d). So we conclude that the spatial variation of EIMC SNR is not caused by the macroscopic heterogeneity of the samples. It might be due to the inherent heterogeneity of EKP.

Also, the SNR was not same in gelatin and porcine heart sample even when they were placed in contact. Electric field was applied on the gelatin sample which was fixed on the top of the porcine heart sample during experiment. The SNR was found higher at some locations in the porcine heart sample which were close to the gelatin sample as shown in the Fig 4.13 (d).

However, after comparing Fig. 4.5(d) and Fig. 4.13 (d), we conclude that the EIMC SNR is directly related to the sample's electro-kinetic properties because there is no significant difference between the EIMC SNR in the heart tissue and the gelatin in both experiment configurations.

In order to further study the effect of electric current through tissues and their characterization, layered tissues were used which consists of three different layers: porcine heart muscle, fat and gelatin sample. In the experiment having only two samples (porcine heart and the gelatin, section 4.3.1), the higher SNR in the gelatin (greater than 1) near the pork boundary and other parts of the gelatin might be due to the flow of current from porcine heart tissue to the gelatin sample and induced mechanical changes on the gelatin sample. It seems no significant difference in SNR between the tissue part and the gelatin part.

Then two experiments were performed by using the porcine heart muscle, fat and the gelatin sample. The experimental results were presented in the section 4.4.1 and 4.5.1. The amplitude of some fat and gelatin windows changes continuously at the same frequency as the applied voltage as shown in the section 4.4.2 and 4.5.2. However, amplitude change is not same for all the windows of the sample during application of electric field, the mean amplitude of the signal at frequency 0.02Hz in porcine heart muscle was found higher (except at some locations in the porcine heart muscle) than in fat and gelatin sample as shown in the Fig 4.7 (b). The SNR in the porcine heart muscle, fat and some parts of the gelatin sample was found greater than one during electric field application as shown in the Fig 4.7 (d) and 4.9 (d).

Electro-kinetic response of biological tissues with optical coherence tomography (OCT) was performed in the previous study in which a 1 mm diameter dielectric optical fiber was inserted

into the middle of the sample [46]. The changes of backscattered OCT signal from porcine heart tissues were investigated with a low frequency AC electric field. The signal-to-noise ratio in the OCT based EIOC image (normalized by the EIOC background image) during electric field application was found small in the fiber and no EIOC of signal in the fiber glass region were detected even though there are significant EIOC in the tissue surrounded it. This is in agreement with this study where thin plastic was used as an insulator to separate the pork heart muscle and the gelatin sample.

In summary, the experiment results show that the concept of SNR can reduce the weight of ultrasound signal amplitude in quantifying the electro-kinetic phenomena in the samples. The SNR is sensitive to the existence of electric current in the samples. The SNR seems not discriminative enough to classify different types of samples.

5.2 Conclusions and Future-work

The effect of electric field in layered tissues and ultrasound phantoms was analyzed by finding the frequency spectra, mean amplitude of the signals, root mean square of the noise and Signal-to-noise ratio. SNR was found to be the best measure to demonstrate the current distribution in tissues and phantoms. The SNR was compared in both cases when the samples were separated and not separated by the insulator (thin plastic). There was significant difference in SNR between the different parts of the sample when there was insulator. However, the difference is much smaller without plastic between samples. For in vitro porcine sample, the SNR in the porcine heart muscle was found larger than in the fat.

Future-work

- In this study, the signal-to- noise ratio was calculated for a single A-line. However, in future the two dimensional method, B-mode ultrasound can be investigated for the better understanding of the SNR in tissue and samples during electric field application.
- Our results show that that the EIMC SNR can indicate the existence of AC electric current in samples, rather than be directly related to the sample's electro-kinetic properties of the samples. In the future study, it would be interesting to investigate quantitatively the dependence of EIMC SNR on the current distribution in the samples. If the current distribution in a sample can be measured, it is possible to reconstruct the electric impedance of the sample, which can provide useful diagnostic information.

References:

[1] F. Simon, "Electrokinetic Phenomena," Leibniz Institute of Polymer Research, Dresden, Germany, 2009.

[2] M. Kaszuba, J. Corbett, F. M. Watson, and A. Jones, "High-concentration zeta potential measurements using light-scattering techniques.," *Philos. Trans. A. Math. Phys. Eng. Sci.*, vol. 368, no. 1927, pp. 4439–4451, Sep. 2010.

[3] J. Mamou, *Quantitative Ultrasound in Soft Tissues*. Dordrecht: Springer Netherlands, 2013.

[4] H. Ammari, *An Introduction to Mathematics of Emerging Biomedical Imaging*, vol. 62. Springer Berlin Heidelberg, 2008, pp. 3–13.

[5] T. L. Szabo, *Diagnostic Ultrasound Imaging Inside Out*. Saint Louis, MO, USA: Elsevier, Academic Press, 2004.

[6] J. M. Sanches, A. F. Laine, and J. S. Suri, *Ultrasound imaging advances and applications*. Springer New York, 2012.

[7] F. M. Abu-Zidan, A. F. Hefny, and P. Corr, "Clinical ultrasound physics.," *J. Emerg. Trauma. Shock*, vol. 4, no. 4, pp. 501–503, Oct. 2011.

[8] P. Laugier and H. Guillaume, *Bone quantitative ultrasound*. Springer New York, 2011.

[9] J. E. Aldrich, "Basic physics of ultrasound imaging.," *Crit. Care Med.*, vol. 35, no. 5 Suppl, pp. S131–137, May 2007.

[10] B. A. J. Angelsen, "A theoretical study of the scattering of ultrasound from blood," *IEEE Trans. Biomed. Eng.*, vol. BME-27, no. 2, pp. 61–67, 1980.

[11] J. K. Seo and E. J. Woo, "Electrical tissue property imaging at low frequency using MREIT," *IEEE Trans. Biomed. Eng.*, vol. 61, no. 5, pp. 1390–1399, 2014.

[12] O. Doganay and Y. Xu, "The effect of electric current in biological tissues on ultrasound echoes," *2009 IEEE Int. Ultrason. Symp.*, pp. 2103–2106, Sep. 2009.

[13] P. C. Miranda, A. Mekonnen, R. Salvador, and P. J. Basser, "Predicting the electric field distribution in the brain for the treatment of glioblastoma.," *Phys. Med. Biol.*, vol. 59, no. 15, pp. 4137–4147, Aug. 2014.

[14] P. H. Lento and S. Primack, "Advances and utility of diagnostic ultrasound in musculoskeletal medicine.," *Curr. Rev. Musculoskelet. Med.*, vol. 1, no. 1, pp. 24–31, Mar. 2008.

[15] Z. Wang, P. Ingram, R. Olafsson, Q. Li, and R. S. Witte, “Detection of multiple electrical sources in tissue using ultrasound current source density imaging,” *SPIE*, vol. 7629, no. 10, p. 76290H–76290H–9, Mar. 2010.

[16] G. Hu, X. Li, and B. He, “Imaging biological tissues with electrical conductivity contrast below 1 S m by means of magnetoacoustic tomography with magnetic induction.,” *Appl. Phys. Lett.*, vol. 97, no. 10, pp. 1–3, Sep. 2010.

[17] K. Dickie, R. Zahihi, L. Pelissier, and C. Leung, “A Flexible Research Interface for Collecting Clinical Ultrasound,” *SPIE*, vol. 7494, no. 2, pp. 130–136, 2009.

[18] J. G. Stinstra and M. Hendriks, “Estimation of the Electrical Conductivity of Human Tissue,” *Electromagnetics*, vol. 9, no. 10, pp. 545–557, 2001.

[19] E. Gilboa, P. S. La Rosa, and A. Nehorai, “Estimating electrical conductivity tensors of biological tissues using microelectrode arrays.,” *Ann. Biomed. Eng.*, vol. 40, no. 10, pp. 2140–2155, Oct. 2012.

[20] D. Miklavcic, N. Pavselj, and F. Hart, “Electric properties of tissues,” *Wiley Encyclopedia of Biomedical Engineering*. John Wiley & Sons, Inc., pp. 1–12, 2006.

[21] B. Roth, “The Electrical Conductivity of Tissues,” in *The Biomedical Engineering Handbook, Second Edition.*, CRC Press, 1999.

[22] I. Llorente, S. Fajardo, and J. M. Bastidas, “Applications of electrokinetic phenomena in materials science,” *J. Solid State Electrochem.*, vol. 18, no. 2, pp. 293–307, Oct. 2013.

[23] S. Wall, “The history of electrokinetic phenomena,” *Curr. Opin. Colloid Interface Sci.*, vol. 15, no. 3, pp. 119–124, Jun. 2010.

[24] D. T. Oakes, “Electrokinetic Phenomena in Colloidal Clays,” *Clays Clay Miner.*, vol. 4, no. 1, pp. 225–239, 1955.

[25] Y. Liu, M. Liu, W. M. Lau, and J. Yang, “Ion size and image effect on electrokinetic flows.,” *Langmuir*, vol. 24, no. 6, pp. 2884–2891, Mar. 2008.

[26] D.-S. Lian and S.-J. Zhao, “Capillary electrophoresis based on the nucleic acid detection in the application of cancer diagnosis and therapy,” *R. Soc. Chem.*, vol. 139, no. 14, pp. 3492–3506, Jul. 2014.

[27] A. V. Delgado, R. J. Hunter, L. K. Koopal, and J. Lyklema, “Measurement and interpretation of electrokinetic phenomena.,” *J. Colloid Interface Sci.*, vol. 309, no. 2, pp. 194–224, May 2007.

[28] B. Salopek, D. Krasic, and S. Filipovic, “Measurement and application of zeta-potential,” *Rud. - Geol. - Naft. Zb.*, vol. 4, no. 1, pp. 147–151, 1992.

[29] W. Y. Gu, W. M. Lai, and V. C. Mow, “Transport of multi-electrolytes in charged hydrated biological soft tissues,” *Transp. Porous Media*, vol. 34, no. 1–3, pp. 143–157, 1999.

[30] X. Zhang, S. Zhu, and B. He, “Imaging electric properties of biological tissues by RF field mapping in MRI.,” *IEEE Trans. Med. Imaging*, vol. 29, no. 2, pp. 474–81, Feb. 2010.

[31] B. Reynaud and T. M. Quinn, “Tensorial electrokinetics in articular cartilage,” *Biophys. J.*, vol. 91, no. 6, pp. 2349–2355, Sep. 2006.

[32] W. D. Comper, *Extracellular matrix*, 1st ed. Amsterdam, Netherland: Harwood academic publishers, 1996.

[33] A. R. Jackson, T.-Y. Yuan, C.-Y. Huang, and W. Y. Gu, “A conductivity approach to measuring fixed charge density in intervertebral disc tissue,” *Ann. Biomed. Eng.*, vol. 37, no. 12, pp. 2566–2573, Dec. 2009.

[34] V. C. Mow, G. A. Ateshian, W. M. Lai, K. Kang, D. N. Sun, and W. Y. Gu, “Effect of fixed charge density on stress-relaxation behavior of hydrated soft tissues in confined compression,” *Orthop. Res. Soc.*, vol. 35, no. 34, pp. 4945 – 4962, 1999.

[35] J. C. Iatridis, J. P. Laible, and M. H. Krag, “Influence of fixed charge density magnitude and distribution on the intervertebral disc: applications of a poroelastic and chemical electric (PEACE) model.,” *J. Biomech. Eng.*, vol. 125, no. 1, pp. 12–24, Feb. 2003.

[36] O. Doganay and Y. Xu, “Electric-field induced strain in biological tissues.,” *J. Acoust. Soc. Am.*, vol. 128, no. 5, pp. EL261–267, Nov. 2010.

[37] B. Szachowicz-Petelska, I. Dobrzyńska, Z. Figaszewski, and S. Sulkowski, “Changes in physico-chemical properties of human large intestine tumour cells membrane.,” *Mol. Cell. Biochem.*, vol. 238, no. 1–2, pp. 41–47, Sep. 2002.

[38] B. Szachowicz-petelska, I. Dobrzynska, S. Sulkowski, and Z. Figaszewski, “Characterization of the cell membrane during cancer transformation,” *J. Environ. Biol.*, vol. 31, no. 5, pp. 845–850, 2010.

[39] I. F. Tannock and D. Rotin, “Acid pH in tumors and its potential for therapeutic exploitation,” *Cancer Res.*, vol. 49, no. 16, pp. 4373–4384, 1989.

[40] K. K. Shung, “Ultrasonic Scattering in Biological Tissues,” *J. Acoust. Soc. Am.*, vol. 94, no. 5, pp. 3033 – 3037, 1993.

[41] K. Nam, G. Ghoshal, and T. J. Hall, “Comparison of ultrasound attenuation and backscatter estimates in layered tissue-mimicking phantoms among three clinical scanners,” *Ultrason Imaging*, vol. 34, no. 4, pp. 209–221, 2013.

[42] J. F. Chen, J. A. Zagzebski, and E. L. Madsen, “Tests of backscatter coefficient measurement using broadband pulses,” *IEEE Trans. Ultrason.*, vol. 40, no. 5, pp. 603–607, Jan. 1993.

[43] V. Chan and A. Perlas, “Basics of ultrasound imaging,” in *Atlas of ultrasound-guided procedures in interventional pain management*, Springer New York, 2011, pp. 13–19.

[44] W. J. Davros, J. A. Zagzebski, and E. L. Madsen, “Frequency-dependent angular scattering of ultrasound by tissue,” *Acoust. Soc. Am.*, vol. 80, no. 1, pp. 229–237, 1986.

[45] J. G. Fujimoto, C. Pitris, S. A. Boppart, and M. E. Brezinski, “Optical coherence tomography : an emerging technology for biomedical imaging and optical biopsy,” *Neoplasia*, vol. 2, no. 1–2, pp. 9–25, 2000.

[46] K. Wawrzyn, V. Demidov, B. Vuong, M. K. Harduar, C. Sun, V. X. D. Yang, O. Doganay, V. Toronov, and Y. Xu, “Imaging the electro-kinetic response of biological tissues with optical coherence tomography,” *Opt. Lett.*, vol. 38, no. 14, pp. 2572–2574, Jul. 2013.

[47] J. R. Cook, R. R. Bouchard, and S. Y. Emelianov, “Tissue-mimicking phantoms for photoacoustic and ultrasonic imaging.,” *Biomed. Opt. Express*, vol. 2, no. 11, pp. 3193–3206, Nov. 2011.

[48] E. L. Madsen, M. A. Hobson, H. Shi, T. Varghese, and G. R. Frank, “Tissue-mimicking agar/gelatin materials for use in heterogeneous elastography phantoms,” *Phys. Med. Biol.*, vol. 50, no. 23, pp. 5597–5618, Dec. 2005.

[49] N. G. Parker and M. J. W. Povey, “Ultrasonic study of the gelation of gelatin: Phase diagram, hysteresis and kinetics,” *Food Hydrocoll.*, vol. 26, no. 1, pp. 99–107, Jan. 2012.

[50] O. R. Seryasat, M. A. Shoorehdeli, H. Honarvar, and A. Rahmani, “Multi-fault diagnosis of ball bearing using FFT, wavelet energy entropy mean and root mean square (RMS),” *IEEE*, vol. 1, no. 10, pp. 4295–4299, 2010.

[51] L. Zhang, H. Xu, and M. Gu, “Use of signal to noise ratio and area change rate of spectra to evaluate the Visible/NIR spectral system for fruit internal quality detection,” *J. Food Eng.*, vol. 139, pp. 19–23, Oct. 2014.

[52] Z. Yang, T. K. Sinha, and J. C. Gore, “The influence of tissue composition on signal to noise ratio of MR measurements,” *Intl. Soc. Mag. Reson*, vol. 16, p. 2609, 2008.